NASA TECHNICAL MEMORANDUM

NASA TM 82435

Accommodations Assessment: Spaceborne Doppler Lidar Wind Measuring System

By Program Development
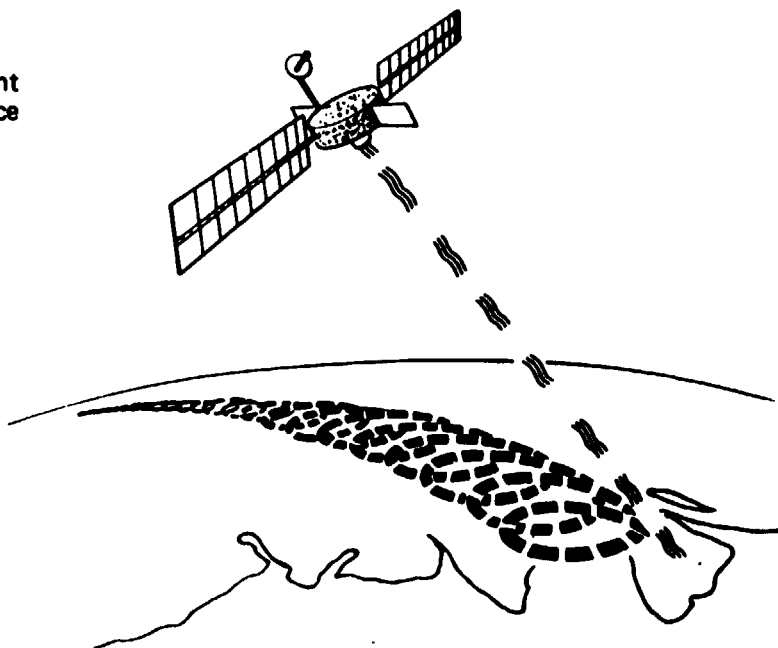Preliminary Design Office

August, 1981

NASA

George C. Marshall Space Flight Center
Marshall Space Flight Center, Alabama

ACCOMMODATIONS ASSESSMENT
SPACEBORNE DOPPLER LIDAR
WIND MEASURING SYSTEM

CONTENTS

The assessment activities summarized here were performed by the below-named members of the MSFC Preliminary Design Office (PD01). However, it is appropriate to acknowledge the assistance of Mr. J. Bilbro (EC32) relative to the characteristics and principles of doppler lidar wind measuring systems. Also, Mr. R. Beranek (PS06) provided guidance to the over-all assessment of which these PD01 activities were a part.

J. STEINCAMP, PD34, ENGINEERING STUDY MANAGER

J. HOWELL, PD12, SUBSYSTEMS LEAD ENGINEER/ATTITUDE DETERMINATION
            AND CONTROL

D. STRIDER, PD23, SYSTEMS LEAD ENGINEER/CONFIGURATION

W. FINNELL, PD14, COMMUNICATIONS & DATA MANAGEMENT

W. JOHANSON, PD24, MASS PROPERTIES

D. MERCIER, PD33, STS PERFORMANCE

J. PEOPLES, PD22, THERMAL ANALYSIS

R. ROOD, PD14, ELECTRICAL POWER

T. WHEELER, PD32, ATMOSPHERIC ENVIRONMENT

A. YOUNG, PD32, FLIGHT PERFORMANCE

D. WALTON, PD32, DOCUMENTATION

LIST OF FIGURES

LIST OF FIGURES (CONTINUED)

I.   INTRODUCTION

I.   INTRODUCTION

I.A.   BACKGROUND AND SCOPE

This document summarizes the activities carried out by the MSFC Preliminary Design Office as part of the NASA assessment of a spaceborne doppler lidar wind measuring system concept. The assessment was requested by Dr. Ron Greenwood, Director of the Environmental Observation Division, Office of Space and Terrestrial Applications, of NASA Headquarters, who designated MSFC as the lead center, to be supported by JPL, LaRC, and GSFC in selected disciplines augmenting MSFC's experience in ground and airborne pulsed CO_2 doppler lidar wind measuring systems.

The assessment activity was organized to concentrate on three areas vital to concept feasibility:

o   Laser and optical systems (Lidar system hardware)

o   Atmospheric characteristics

o   Spacecraft Accommodations

with corresponding assignments of responsibilities to the MSFC Optical and RF Systems Division, Atmospheric Sciences Division, and Preliminary Design Office. Overall assessment coordination was provided by the MSFC Advanced Studies Office.

The system concept under consideration was defined in three reports:

1)   "Feasibility Study of Satellite - Borne Lidar Global Wind Monitoring System", NOAA Tech. Memo ERL WPL-37 (1978)

2)   "Feasibility Study of Satellite - Borne Lidar Global Wind Monitoring System, Part II", NOAA Tech. Memo ERL WPL-63 (1980)

3)   NOAA LMSC WINDSAT Study, Final Briefing Charts (Sep 1980) Contract NA 79 RAC 00127

The LMSC study was managed by the NOAA Environmental Resources Laboratory and funded by the USAF Space Division. All three studies emphasized a Shuttle-borne system, which was considered an evolutionary step in the development of an operational system.

A "clean sheet" approach to spacecraft conceptual design was taken to provide the greatest flexibility in accommodating the mission equipment requirements. This seemed particularly appropriate in view of the electrical power requirements, which would require significant modification of existing spacecraft. Figure I.A-1 is an artist's concept of the operational system.

I.B. ACCOMMODATIONS ASSESSMENT CONCLUSIONS/ RECOMMENDATIONS

Subject to the three caveats following, the principal conclusion of this assessment is that a spacecraft with the capabilities needed to support the operation of the doppler lidar wind measuring system is technically feasible. Cost estimates prepared for a dedicated, new-development spacecraft (using standard, available, and/or existing technology components) suggest economic feasibility of such a spacecraft. Such a new development may be unnecessary: the present assessment did not include detailed consideration of the potential use of existing and "in-development" spacecraft and platforms. The caveats are that

1) cryogenic cooling of the photodetector will not be required in the operational system,

2) detailed structural/pointing analyses will establish feasibility of short-term optical axis stability for efficient lidar heterodyning, and

3) laser power requirements will not increase beyond those now anticipated by more than a factor of three.

The structural and pointing specialists consulted were of the opinion that an acceptable short-term stability could be realized, but that proof of their opinion would require analyses beyond the scope of the assessment. The laser power requirements are a critical design driver: the spacecraft conceptualized in this assessment will not be adequate if the laser power requirement increases much beyond the assumed range of 2140-2340 W. Since the laser power requirement is most particularly determined by atmospheric backscatter, better knowledge of this parameter is required to adequately scope the spacecraft definition activity.

The uncertainty relative to atmospheric backscatter, together with the need for demonstration of adequate laser lifetime and chirp (intra-pulse frequency stability) characteristics, were key considerations in the formulation of the schedule recommendation shown in Figure I.B-1. In

7

DOPPLER LIDAR
WIND MEASURING SPACECRAFT
Figure I.A-1
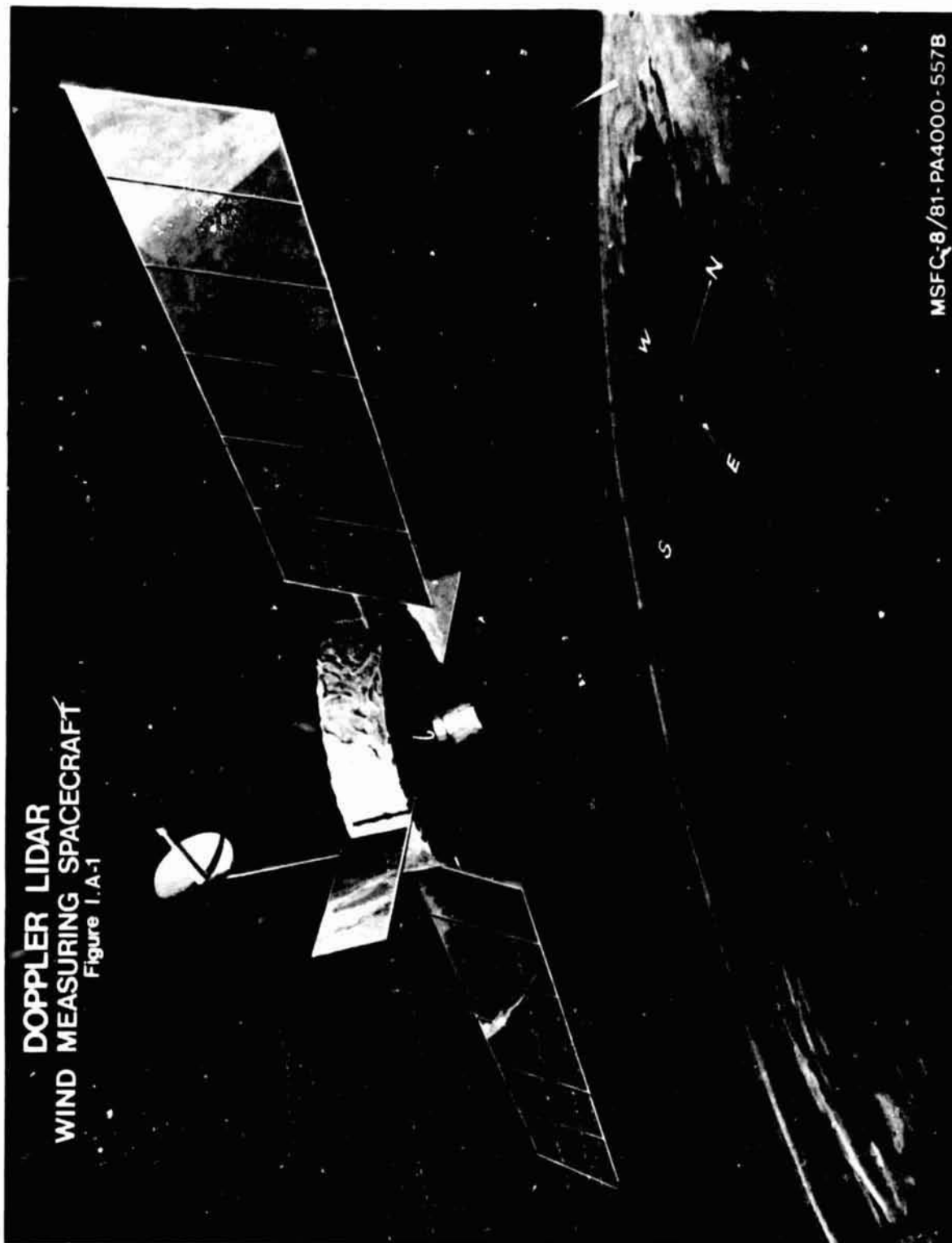
MSFC-8/81-PA4000-557B

FIGURE I. B-1
PROGRAMMATIC SCHEDULE

FY | 81 | 82 | 83 | 84 | 85 | 86 | 87 | 88 | 89 | 90

ASSESSMENT

TECHNOLOGY PHASE

DEMONSTRATION PHASE

OPERATIONAL DEMONSTRATION PHASE

φ (A)   φ (B)   φ (C/D)
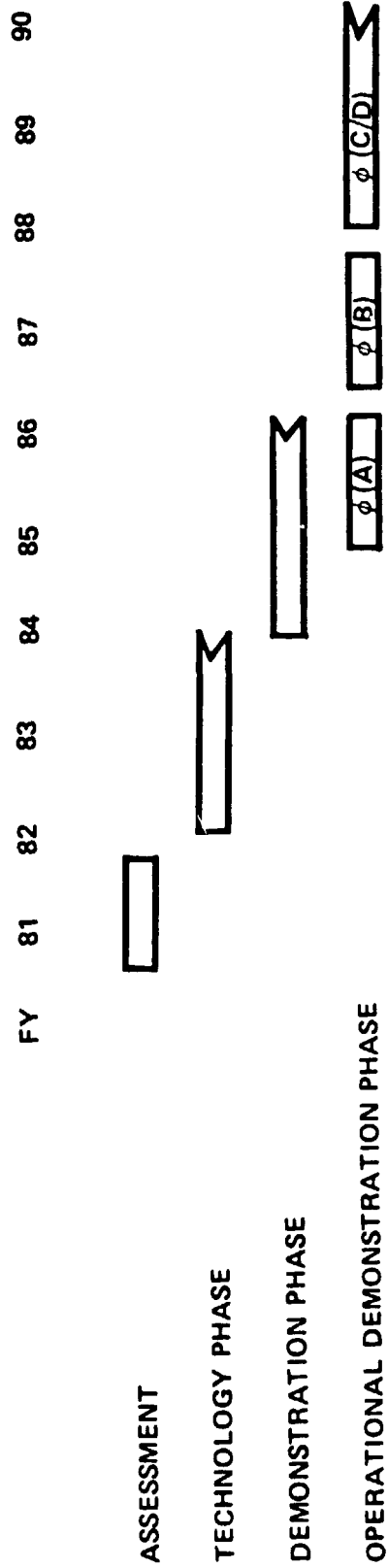
KEY DECISION POINTS

WITHIN 18 MONTHS:
PRELIMINARY BACKSCATTER CRITERIA DEFINITION
CHIRP REQUIREMENTS DEMONSTRATION
LASER CONFIGURATION SELECTION
PRELIMINARY SYSTEM LIFETIME FEASIBILITY DETERMINATION

WITHIN 3–5 YEARS:
BACKSCATTER CRITERIA FINALIZATION
SYSTEM LIFETIME DEMONSTRATION
WIND MEASUREMENT TECHNIQUE DEMONSTRATION

9

particular, a phased hardware development program should be initiated after technology studies yield adequate definition of system requirements.

System studies should continue at an appropriate level to provide guidance to the technology studies and to evolve system requirements. The needs for ground truthing and observations of localized meterological phenomena should be defined as early as possible, as these needs may become design drivers.

I.C   MISSION OBJECTIVES: WIND MEASUREMENT NEEDS

The ultimate objective is that of improving the accuracy of weather forecasting, particularly numerical forecasting. A spaceborne doppler lidar wind measuring system will contribute to this end by providing direct measurement of wind profiles. Two mission objectives have been identified through discussions with NOAA, USAF, and NASA personnel.

> Objective I :   Provide frequent, accurate, and extensive measurements

> Objective II: Provide intensive local observations

The second objective is required to some extent for ground truthing; apart from this, a desirable aim is the observation of localized meteorological phenomena.

Table I.C.1 provides seven goals which may be used to quantify the mission objectives.

TABLE I.C.1 MISSION OBJECTIVES/GOALS

GOAL	OBJECTIVE I QUANTIFICATION	OBJECTIVE II QUANTIFICATION
1. OBSERVATION INTERVAL	3-12 HRS	ON DEMAND-?
2. AREAL COVERAGE	TROPICS-GLOBAL	TEMP-GLOBAL
3. VERTICAL RANGE	10-20 KM	UNSPECIFIED
4. RESOLUTION, VERTICAL	1 KM	UNSPECIFIED
5. RESOLUTION, HORIZONTAL	100-500 KM	10 KM
6. ACCURACY: SPEED	1-2 M/S	UNSPECIFIED
7. ACCURACY: DIRECTION	± 10 DEG	UNSPECIFIED

The first goal relates to the frequency with which the wind fields are updated, and this, in turn, determines the number of spacecraft in the operational system. To visualize this, imagine a single Lidar spacecraft in a polar orbit, being over a point X on the equator at local dawn. Twelve hours later this point will be beneath the spacecraft if it has completed a half-integral number of orbital revolutions - and the winds at point X will be observed again. For this situation, the first physically realizable solution occurs at 7.5 revolutions per half-day, corresponding to an orbital altitude of 570 KM. A lesser number of half-integer revolutions per half-day would require a spacecraft altitude exceeding 1200 KM, where STS performance limitations, Van Allen belt radiation and the strength of the returning Lidar pulse become expensive design drivers. If a second spacecraft is now placed in a polar orbit at the same altitude, oriented and phased to cause the spacecraft to pass over the point X at local noon, then the system of two spacecraft can update the winds at a point X every six hours. Similarly, three spacecraft are required to update at four hour intervals, six are required for three hour updates, and so on.

The second goal, coverage, describes the portion of the Earth's surface over which winds are to be measured. To ensure that winds are measured at all points around the equator according to the observation interval chosen, each spacecraft must measure winds along a swath extending some distance to either side of its ground track. To deduce the total swath width, consider again the case of a single spacecraft in a polar orbit, and not let point X be at the western edge of the measurement swath. It is easy to see that measurement of winds along the equator will be complete if the point X is on the eastern edge of the swath one orbital

11

period later. Using the orbital period already calculated, the total swath width is readily shown to b about 2700 KM. Note that this value results from assuming that there are no measurement gaps along the equator, and so is independent of the observation interval. Further note that, although winds along the equator are measured exactly once during the observation interval, winds in the temperate and artic regions are measured more frequently due to the overlapping measurement swaths in these zones. In this connection, there is a circumstance which may be expected to figure in any future doppler lidar wind measurement system trade studies: tropical winds cannot be deduced reliably from temperature and pressure measurements owing to the sm 1 gradients of these parameters in the tropics. Elsewhere, direct wind measurements can improve on present methods. In the polar zones, above a few kilometers, the signal-to-noise ratio (SNR) of the returning lidar pulse is less than at other latitudes, which tends to reduce the attainable accuracy. However, the overlapping swaths just described provide more measurements, and this slightly offsets the accuracy reduction.

The third and fourth goals, vertical range and resolution, relate to the altitudes to which, and vertical spacings at which, winds can be measured. A 1 KM vertical resolution means that the average horizontal wind is to be estimated in each 1 KM "slab", up to the vertical range. The vertical resolution is limited by the lidar pulse length, the "least reasonably conceiveable value" being about 400 KM (this does not suggest that so fine a vertical resolution is economically attainable, or even meteorologically useful). The strength of the returning lidar pulse depends on the backscatter from atmospheric aerosols-whose concentration must ultimately decrease with altitude and vary with geographic location, season, time of day, and occurrence of aerosol-producing events (e.g., dust storms and volcanic activity). This implies that the maximum altitude from which useful returns will be obtained will vary with all these factors. Thus, the lower figure of 10 KM given for the vertical range should be taken as indicative of a need for measurement of winds up to the tropopause (whose height varies with season and latitude), while the upper figure suggests the utility of stratospheric wind measurements.

The fifth goal, horizontal resolution, derives from two circumstances. First, present numerical weather models operate with geographic grids in which the mean wind over the grid (in each vertical resolution element) is used. Second, only the radial component of wind along the lidar pointing direction can be measured from each pulse (again, in each vertical resolution element). Thus, it is necessary to direct several lidar pulses at a given geographical area, from different directions, to estimate the mean wind by vector resolution. The area, or grid, is usually taken to be square, and the horizontal resolution is the length of the grid side. The lower figure of 100 KM would be representative of small area (fine mesh) modeling. The upper figure of 500 KM would be associated with hemispheric or global modeling. This discussion implies that the flow of data from a doppler lidar wind-measuring spacecraft is not well matched to conventional large-area numerical forecasting models whose world- view requires regular grids and synoptic measurements. This mis-match poses no insurmountable mathematical or physical problem, but does indicate the need for model development to effectively exploit the wind data. The relationship of the data produced and the using models should be factored into future systems engineering studies.

The sixth and seventh goals, accuracies, describe the accuracy with which mean grid winds are to be measured. The values given are slightly more stringent than the accuracies attained when winds are calculated from temperature and pressure measurements.

As noted at the start of this Section, a space-borne doppler lidar is expected to improve numerical weather forecasting by providing direct wind measurements on a global scale. It seems likely that the flow of data from such a system, with some additional ground and/or onboard processing, would permit inference of other atmospheric dynamic parameters (e.g., cloud cover characteristics). The information so gained would not only enhance the contribution to forecasting, but also serve to advance understanding of atmospheric processes. This assessment has focused on the practicability of, and requirements for, accommodating a lidar system on a free-flying operational spacecraft, with some limited consideration of other accommodations possibilities. Not addressed was the possibility of accommodating additional meteorological sensors which, operated in conjunction with a doppler lidar, would provide an even greater contribution to the ultimate objective and, possibly, understanding of atmospheric processes. Both possibilities-fuller exploitation of doppler lidar data and complementary sensors – should be considered in future studies.

13

Certain simplifying assumptions were made above to illustrate the concepts of fleet sizing and swath widths. The precise assumptions (e.g., polar orbits) and parameters based thereon (e.g., 570 KM orbital altitude) are not necessarily required in practice. The conclusions about the required fleet size remain valid.

I.D. MISSION TECHNIQUE: PRINCIPLES OF WIND MEASUREMENT

The word "lidar" was originally an acronym for "Light Detection and Ranging" - i.e., a lidar is a radar operating at optical frequencies. In the system under consideration, a pulse of light of a few microseconds duration, at an essentially constant frequency, is directed at a geographically-fixed volume of the atmosphere. Particles (aerosols) in the volume reflect (backscatter) a portion of the pulse energy back along the direction of propagation of the pulse. This energy is collected at the system and its frequency compared to the frequency of the emitted pulse by optical heterodyning. The relative velocity between the system and the aerosols (or, more precisely, the relative velocity component along the direction of propagation) is defined by the frequency difference, caused by the doppler effect.

The motion of the Earth in inertial space is calculable, and the motion of the spaceborne lidar system can be determined by use of the global positioning system (GPS). The attitude of the spacecraft will be maintained by the onboard inertial reference subsystem. With this information and knowledge of the beam pointing direction, the doppler frequency shift due to spacecraft-Earth motion can be factored out of the total shift, with a remainder due only to the component of aerosol motion along the beam pointing direction. If the aerosols are assumed to move with the wind, then the component of wind motion along the beam pointing direction has been determined. If the wind field in the atmospheric volume is uniform, then directing several pulses into the volume from different points on the orbit permits determination of the wind components by vector resolution along the different beam pointing directions. Although the assumption of wind field uniformity over the atmospheric volume does not always hold, particularly when the volume corresponds to the larger horizontal resolution elements, the nonuniformity does not compromise the concept, as only the mean wind in the volume is sought. In the usual case, it may also be assumed that vertical winds are negligible: the exceptions are generally localized and/or transient phenomena.

14

Figure I.D.1, adapted from the NOAA/LMSC WINDSAT final briefing package, illustrates a doppler lidar wind-measuring system concept. The primary "TEA" (Transversely Excited, Atmospheric)laser output pulses are reflected by an optomechanical switch in the "transmit" positon through a beam alignment subsystem consisting of a fold mirror, a two-axis gimbaled mirror, and a LAC (Lag Angle Compensating) mirror. The pulse is then reflected from the tertiary mirror into the cassegrainian telescope, which expands the beam and directs it at the atmosphere. The pointing direction in this concept is controlled by rotating the telescope about the local vertical at an offset scan angle. In principle, this rotation can be either continuous or stepped.

The returning pulse of backscattered light is collected by the cassegrainian telescope and reflected by the tertiary mirror through the beam alignment subsystem, which directs it through the "receive" position of the switch. The beam alignment subsystem corrects the misalignment due to Bradley abberation caused by the spacecraft motion and, if the rotation is continuous, for the rotation of the telescope (lag angle) during the pulse roundtrip time (typically between 5 and 10 milliseconds). After passing through the switch, the returning light is mixed with a frequency-offset beam from a local oscillator laser by a combining beamsplitter. The offset permits the sense of the doppler shift (red or blue) to be determined. The frequencies of both the local oscillator and the TEA laser are controlled by the technique of injection locking.

The mixed light from the combining beam-splitter forms an interference pattern on the photo-detector. This pattern varies with the doppler-shifted frequency of the returning light. Thus, the detector output is an FM-modulated electrical signal whose modulation frequency corresponds to the doppler shift. The predictable shift due to the spacecraft-Earth motion will vary by about ± 1.7 GHz, depending on whether the beam pointing direction is along or against the spacecraft velocity vector. The function of the frequency synthesizer is the removal of this "gross" doppler shift. The resulting signal is then digitized and range-gated (corresponding to the vertical resolution elements) and, after further preprocessing to extract signal character-istics, recorded for later downlinking.

FIGURE I. D-1
LIDAR SYSTEM CONCEPT
(LASER & OPTICAL SUBSYSTEMS)

16
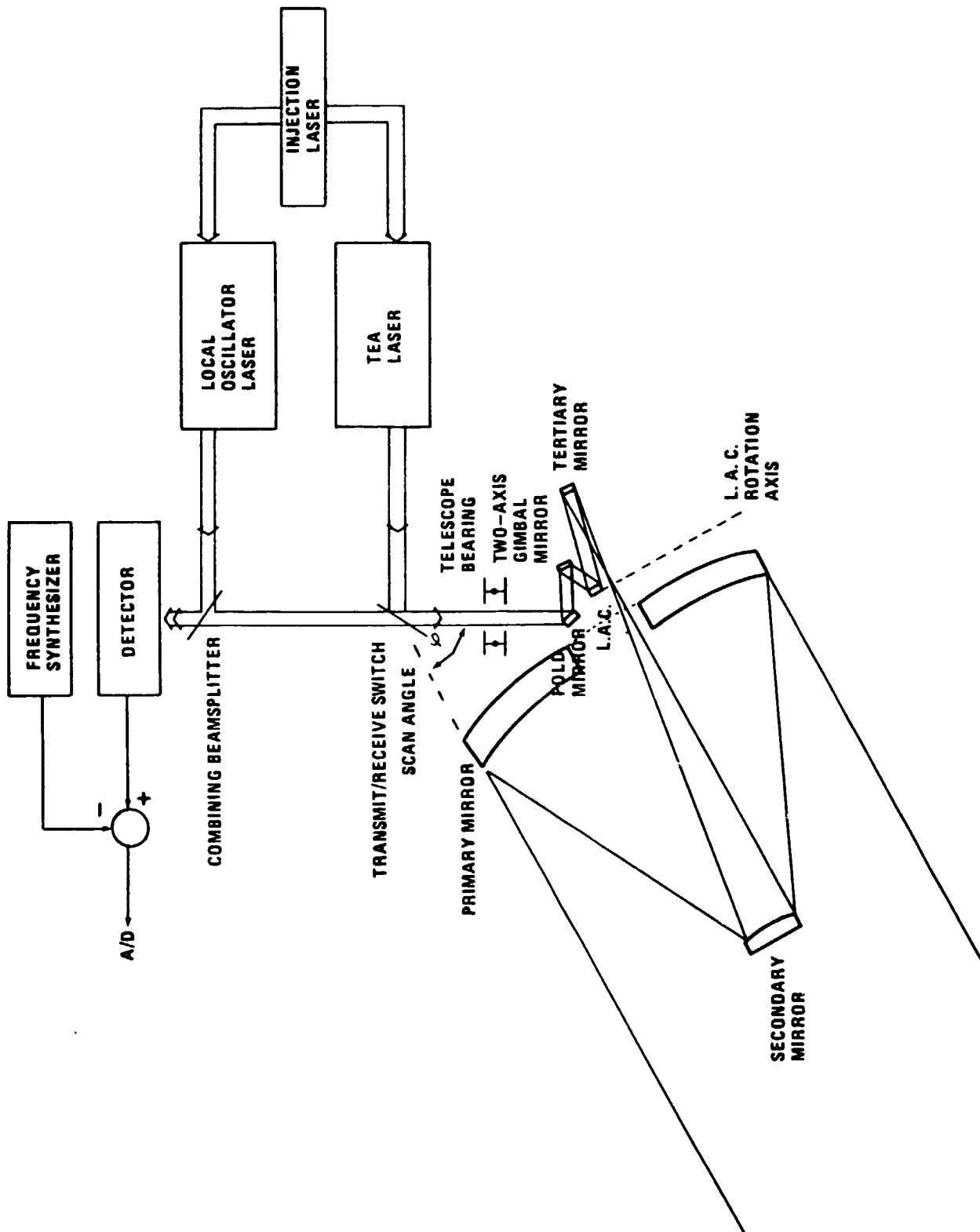
II.   SYSTEM PERFORMANCE ANALYSIS

II.A. SIGNAL-TO-NOISE RATIO

As noted in Section I.C., a primary system performance goal is wind speed measurement accuracy. It is intuitively reasonable that this will improve with increasing values of the signal-to-noise ratio (SNR) of the return pulse. Further, it is reasonable to expect an expression for the SNR of the return from a volume of atmosphere to contain terms involving 1) the output pulse characteristics (energy, duration, and wavelength), 2) atmospheric effects (backscatter, attenuation, and turbulence) and 3) geometry of the collecting optics.

The wind measurement accuracy analyses of WPL-63 are based upon the expression

$$\text{SNR} = \frac{\pi}{8h} \; J\lambda\tau \cdot \beta e^{-2\mu R} \cdot \eta \; \frac{KD^2}{R^2\left(1 + \frac{D}{r_a^2}\right) + \left(\frac{\pi D^2}{4\lambda}\right)\left(1 - \frac{R}{f}\right)^2}$$

where

h = Planck's constant

J = pulse energy

λ = doppler-shifted wavelength

τ = pulse duration

β = atmospheric backscatter coefficient

μ = atmospheric attenuation coefficient

R = range from spacecraft to atmospheric volume

η = overall detector-optics efficiency

D = telescope diameter

r_a = turbulence-induced transverse coherence radius

   = $0.069 \; \lambda^{6/5} \; (RC_n^2)^{-3/5}$

C_n^2 = refractive index structure parameter

f = focal length

In fact, the SNR should be written as a function of the altitude from which the return occurs: letting

a = altitude of the sampled volume

Δa = vertical resolution

α = scan angle

18

$h_{s/c} =$ spacecraft altitude

$R = R (h_{s/c}, \alpha; a)$

$=$ range from spacecraft to altitude at scan angle

The expression $\beta e^{-2\mu R}$ is more accurately written as

$$\frac{dR(h_{s/c}, \alpha; a)}{da} \Delta a \cdot \beta(\lambda, a) \cdot exp\left\{-2 \int_a^{h_{s/c}} \mu(\lambda, x) dR(h_{s/c}, \alpha; x)\right\}$$

where the form of the integral indicates that the attenuation is evaluated along the line connecting the spacecraft and the volume. A similar modification for the turbulence radius is implied (cf. WPL-37, P.203).

For the present purpose of assessing the accommodations required for a wind measuring doppler lidar system, a simpler form of the SNR expression will suffice, and the following expression has been used:

$$SNR (a) = \left[\frac{1}{h} J \lambda \tau\right]\left[\beta(a) \cdot exp\left\{-2 \int_a^{h_{s/c}} \mu(x) dR(h_{s/c}, \alpha; x)\right\}\right] \cdot \gamma \left[\frac{D}{R(h_{s/c}, \alpha; a)}\right]^2$$

Figure II.A-1 displays the result of one calculation using this expression. The assumptions relative to atmospheric attenuation and backscatter are discussed in the next section.

II.B. ATMOSPHERIC UNCERTAINTIES

Ultimately, the feasibility of accommodating the proposed wind-measuring system will depend on atmospheric properties, particularly attenuation and backscatter. The total attenuation can be expected to be only slightly greater than the molecular absorption, particularly above about 7 KM. Figure II.B-1 plots the molecular absorption coefficient at the 9.1145μ wavelength for the AFGL model atmospheres. Although the absorption at a specific altitude and place will vary with time-of-day, season, and weather, the vari- ability is reasonably well bounded. The form of the attenuation term in the SNR expression implies that long light paths through the atmosphere should be avoided.

The uncertainty associated with the backscatter is much less well understood. Figure II.B-2 is a compendium of backscatter estimates from various wavelengths other than the ones of interest, with considerable reliance on the aerosol size distribution models. In this report, calculations have been based on the assumed "worst case" curve. The presence of Lidar returns does indicate the basic feasibility of the doppler lidar wind measuring technique.

FIGURE II. A-1
SIGNAL-TO-NOISE RATIO VS. ALTITUDE

ORBITAL ALTITUDE = 650 (KM)
ORBITAL INCLINATION = 57 (DEG)
OPTICS DIAMETER = 1.25 (M)
WAVELENGTH = 9.1145 (MICRO M)
ATTENUATION = AFGL TROPICAL ABSORPTION
BACKSCATTER = MSFC WORST CASE
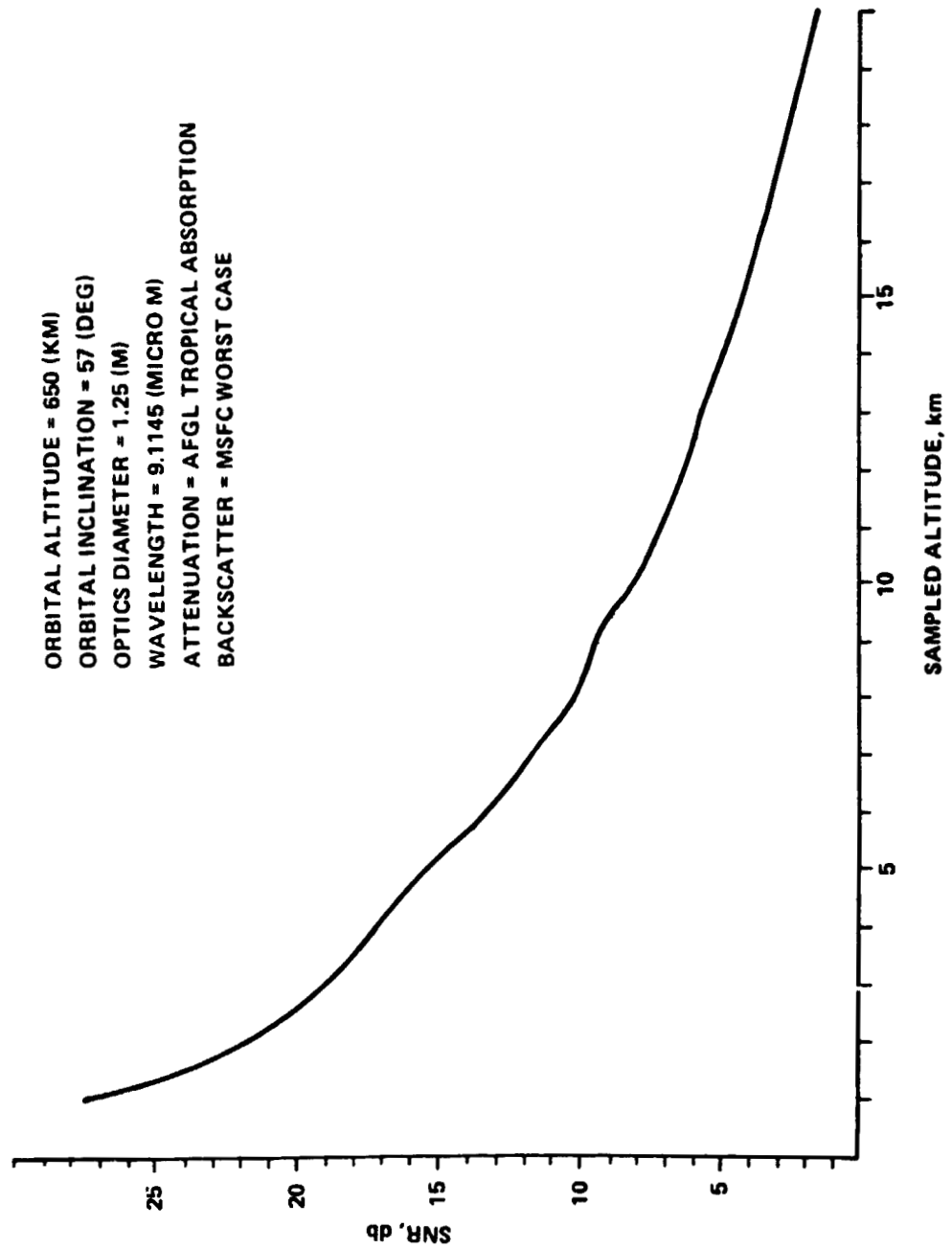
Clearly, an operational system will not be able to measure winds at all altitudes, at all times: clouds are one inhibiting factor, and there will be occasions when the concentrations of aerosols in some regions and at some altitudes will be insufficient to provide a useful return signal.

FIGURE II. B-1
MOLECULAR ABSORPTION COEFFICIENT (km^{-1})
ATλ = 9.1145 μm
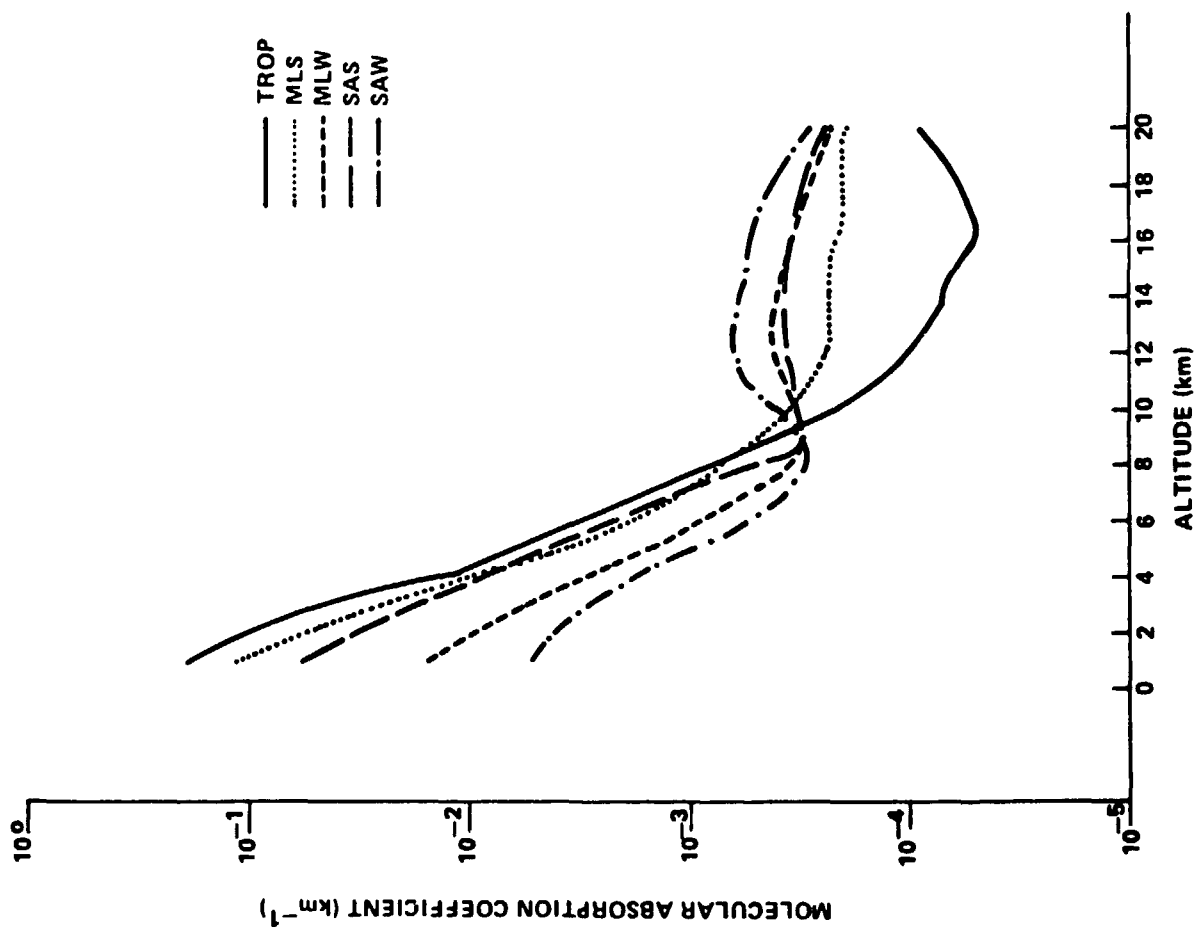
FIGURE II. B-2

IR BACKSCATTERING COEFFICIENT AS A FUNCTION OF ALTITUDE

+ TROPICAL (AEROSOL MODEL)
* MID LATITUDE SUMMER (AEROSOL MODEL)
◇ MID LATITUDE WINTER (AEROSOL MODEL)
| SUBARCTIC SUMMER (AEROSOL MODEL)
X SUBARCTIC WINTER (AEROSOL MODEL)
□ 10.6 μ DUSTSONDE
▲ TOON & POLLACK (9.1 μ)
● TOON & POLLACK (10.6 μ, 11.1 μ)

～ SCHOTLAND (EXTRAPOLATED TO 10.6 μ)
O SCHWIESOW MEDIAN (10.6 μ)
╫ SCHWIESOW MEASUREMENT RANGE
═ MSFC LIDAR SENSITIVITY (10.6 μ)
□ MSFC X DETECTION DURING AIRBORNE TESTS
••• FIREPOND MEASUREMENT (10.6 μ)
▩ GASP (AEROSOL SAMPLE)
△ MSFC GROUND MEASUREMENT (10.6 μ)

SOME OF THIS DATA WAS TAKEN FROM NOAA REPORTS WPL-37 AND WPL-43

23

III. CONFIGURATION AND MASS PROPERTIES

III. CONFIGURATION AND MASS PROPERTIES

III.A. REQUIREMENTS AND ASSUMPTIONS

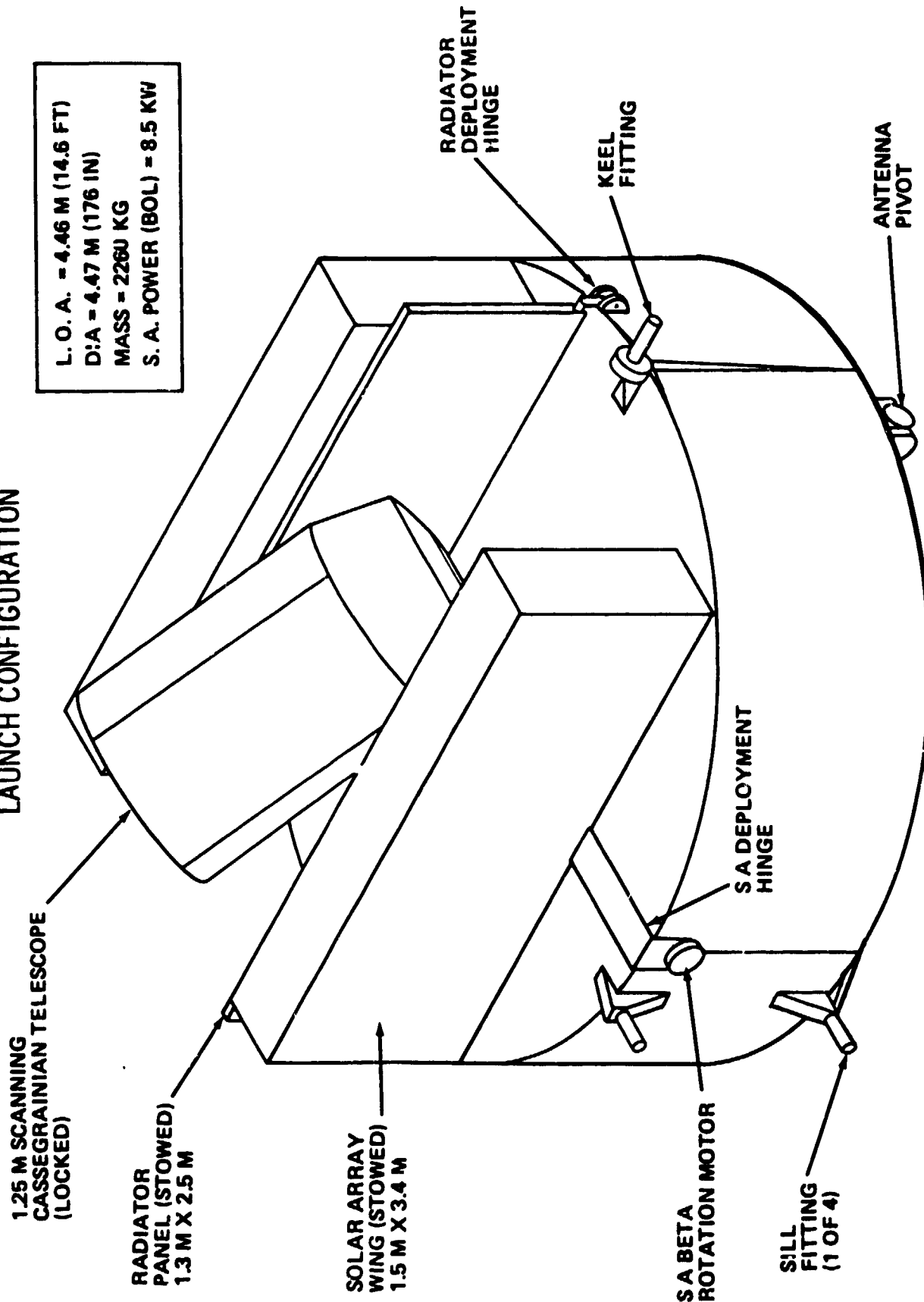The following assumptions and requirements determined the configuration design approach

(i)   Beam pointing shall be realized by a scanning Cassegrainian telescope with a maximum diameter of 1.25 m. The scanning axis shall be aligned with the local vertical, and the optical axis of the telescope shall be offset by approximately 56 deg (the scan angle). The scan rate shall be approximately 4 rpm.

(ii) The Shuttle shall be the launch vehicle, and the spacecraft shall be retrievable

(iii) There shall be two solar array wings of approximately 28m^2 individual area, capable of both deployment and retraction.

(iv) There shall be two deployable/ retractable radiators (both sides active) with total area of approximately 5.7m^2

The mission equipment (laser, scan mechanism, and telescope) was assumed to be similar to the continuously scanning, one-meter, Cassegrainian configuration reported in the NOAA/LMSC WINDSAT Final Briefing Charts: a fritted glass mirror was assumed rather than the Beryllium mirror recommended by LMSC.

III.B. CONCEPTUAL DESIGN

Figure III.A-1 illustrates the features of the conceptual configuration, as it would be stowed in the orbiter cargo bay. The cylindrical spacecraft has the maximum diameter compatible with the orbiter cargo bay dynamic envelope and a height of 1.5 m. The resulting internal volume easily accommodates the mission and subsystems equipment, as determined by a trial layout. This "pancake" configuration is the result of a natural tendency to effectively utilize the cargo bay volume: it does not, in this instance, result from the present commercial payload STS charge policy. The driving cost factor under this policy according to performance calculations, would be the weight delivered to orbit

FIGURE III. A-1
DOPPLER LIDAR WIND MEASURING SPACECRAFT
LAUNCH CONFIGURATION

L.O.A. = 4.46 M (14.6 FT)
D:A = 4.47 M (176 IN)
MASS = 2260 KG
S. A. POWER (BOL) = 8.5 KW

RADIATOR DEPLOYMENT HINGE

KEEL FITTING

ANTENNA PIVOT

S A DEPLOYMENT HINGE

1.25 M SCANNING CASSEGRAINIAN TELESCOPE (LOCKED)

RADIATOR PANEL (STOWED) 1.3 M X 2.5 M

SOLAR ARRAY WING (STOWED) 1.5 M X 3.4 M

S A BETA ROTATION MOTOR

SILL FITTING (1 OF 4)

PD/23 STRIDER

26

rather than payload length. The antenna feed horn is stowed in the body of the spacecraft when the antenna is retracted: a foldable horn could also be used to minimize the stowed payload length.

The keel and sill fittings attach to the payload primary structure, obviating the need for a separate launch cradle. This integration of the launch cradle into the spacecraft is not only programmatically simpler, it also minimizes the total payload- chargable cargo mass. In doing so, it permits consideration of direct delivery to orbit (at 57 deg) without use of an upper stage or an integral propulsion system for orbital transfer (at least one, and likely two, orbiter OMS kits would be required otherwise). This is not to suggest that this will ultimately be the preferred approach, only that this is one option. The sill fittings are spaced 59 inches apart (as on a standard ESA pallet) to provide the maximum number of possible attach positions in the cargo bay. A grapple fixture (not shown) is provided to allow deployment/ retrieval using a remote manipulator arm.

The telescope, radiators, and folded solar arrays are mounted on one flat side of the "pancake" spacecraft and secured by launch locks. The radiators rotate 180 deg during deployment into the position illustrated in the artists' concept in Figure I.A-1. Similarly, the solar array wings are mounted on short arms and rotate 180 deg about the illustrated hinge points before unfolding to their operational position. The antenna is mounted on the remaining flat side of the spacecraft.

III.C.   SYSTEM SIZING

Subsystem and spacecraft mass estimates are given in the following Table: these masses are based on the mission equipment masses taken from the NOAA/LMSC WINDSAT Study Final Briefing Charts, subsystem mass estimates, and the assumption of an all- aluminum spacecraft structure.

TABLE III.C-1

DOPPLER LIDAR WIND MEASURING SYSTEM

PAYLOAD MASS SUMMARY

LIDAR MISSION EQUIPMENT	610 Kg
STRUCTURE	500
ATTITUDE CONTROL AND DETERMINATION	150
COMMUNICATIONS AND DATA MANAGEMENT	80
ELECTRICAL POWER	820
THERMAL CONTROL	90
	2260

IV.   SUBSYSTEMS

IV.A. ELECTRICAL POWER SUBSYSTEM

IV.A.1 REQUIREMENTS AND ASSUMPTIONS

Conceptual design and analysis of the electrical power subsystem requires definition of the loads (power and voltage), orbit (altitude and inclination), and mission factors such as mission duration and spacecraft pointing.

For the doppler lidar wind measuring system spacecraft, the loads were estimated as:

Guidance and Navigtion	227	– 247 W
Communications and Data Management	110	– 115 W
Thermal Control		360 W
Mission Equipment	<u>2140</u>	– <u>2346 W</u>
Totals	2827	– 3068 W

The subsystem estimates are based on representative equipment selections by subsystem engineers. The thermal control power requirement is highly conservative, being based on the startup power for a gas pump. The mission equipment power estimates were taken from the September 1980 NOAA/LMSC WINDSAT Final Briefing Charts.

A design margin of 15-25% is customary in preliminary design activity to allow for uncertainties which almost invariably lead to growth in power requirements as the design matures. Using 3500 W as the total electrical power requirement yields a 24% and a 14% margin relative to the low and high estimates, respectively, of the last paragraph. On balance, this estimate is slightly more conservative than usual. The EPS design is not sensitive to small departures from this value, whose adoption obviates the unenlightening production of many tables and equipment lists tailored to minor differences in the cases considered.

The choice of orbit has two primary effects upon EPS design: first, the solar array and battery system must be sized to supply exlipse loads; second, the altitude, inclination, and launch date (within the solar cycle) affect the particulate radiation, which degrades the solar array. A lower orbit gives a lower light/ dark ratio (requiring a larger array and battery system) whereas a higher orbit yields greater radiation damage due to geomagnetically trapped particles. For this study, a three-year mission coinciding

with a peak period of solar activity was assumed, so that flare protons were a major contributor to the array degradation.

Five orbits were analyzed to scope the characteristics of a conceptual EPS design:

ORBIT #	ALTITUDE (km)	INCLINATION (deg)	NODE (hr)
1	800	sun-synch	0600
2	650	sun-synch	0600
3	800	sun-synch	1200
4	800	57	any
5	500	57	any

The first and third of these represent the best- and worst-cases, respectively, for a high-inclination, 800 km orbit (as per the NOAA WPL-37 and -63 reports). The 0600 node maximizes the day/night ratio (yielding the "minimum" EPS) while the 1200 node has the opposite effect. The second orbit was analyzed to assess the sensitivity of the EPS to orbital altitude at the most favorable nodal position. The fourth and fifth orbits were analyzed to bound the EPS characteristics in orbits potentially accessible from KSC: nodal position is not an EPS driver at the 57 deg inclination.

IV.A.2. CONCEPTUAL DESIGN

The relatively large power requirement of 3500 W and the local vertical orientation of the telescope scan axis necessitates an oriented (sun-tracking) solar array. Two rotational degrees of freedom are used to maximize the array output: roll about the scan axis and rotation of the solar arrays. The first of these is compatible with the need to minimize the sunlight incident on the radiators. Rotation of the solar arrays implies use of solar array drive mechanisms and power transfer devices (such as slip rings or flex cables). These solar array components have been developed for many programs, and there is ample experience for the present application.

A variety of power distribution and control schemes are possible: the concept described here is not necessarily optimum, but is adequate to provide estimates of the realizable efficiencies, weights, and dimensions.

Figure IV.A-1 illustrates the concept. Solar array power is transferred via slip rings or flex cables to the main power bus at a nominal 34 Vdc (varying with array temperature). The power control unit (PCU) provides command, control, and protection functions. During the daylight portion of the orbit, the PCU routes solar array power to the battery charge controllers (CCs) which provide a charge/discharge path for the NiCd battery assemblies. The PCU also routes power from the solar array (or battery, at night) to the multiple load buses which, in turn, distribute power to the various users. The load buses interface loads through remotely located distributors which provide local switching, isolation, and protective functions. Note that this distribution scheme distributes unregulated power at 22-34 dc (depending on array temperature and battery state of charge). The various loads must then provide their own power supplies (dc-dc), which is not true for a distribution scheme tailored to the case where all loads require a specific, regulated (usually 28 Vdc) source. In the present application, the lidar is the major power user, requiring high power, high voltage supplies. The regulated bus approach would have the disadvantage of regulating the power twice, yielding a lower overall conversion efficiency.

Figure IV.A-1 indicates optional charge controllers and batteries. This reflects the different energy storage requirements of the candidate orbits. An operational system with several spacecraft at different nodes could have a common power system with different energy storage capacities.

Figure IV.A-2 illustrates the solar array concept, having two identical wings equipped with deploy/retract mechanisms and power transfer/drive mechanisms for sun orientation and power transfer. Each wing consists of a number of submodules for ease of manufacture, assembly, and launch. The submodules are assemblies of solar cells, various terminals, diodes, and harness wiring features. Some submodules also incorporate thermal and current sensors for array diagnostics. Sun sensors on each wing provide the solar orientation signals needed by the solar array drive electronic assembly mounted within the spacecraft.

Power and signals are routed to the spacecraft by a "power system harness".

IV.A.3. SYSTEM SIZING

The first step in system sizing is the determination of the end-of-life solar array power requirement and

FIGURE IV. A-1
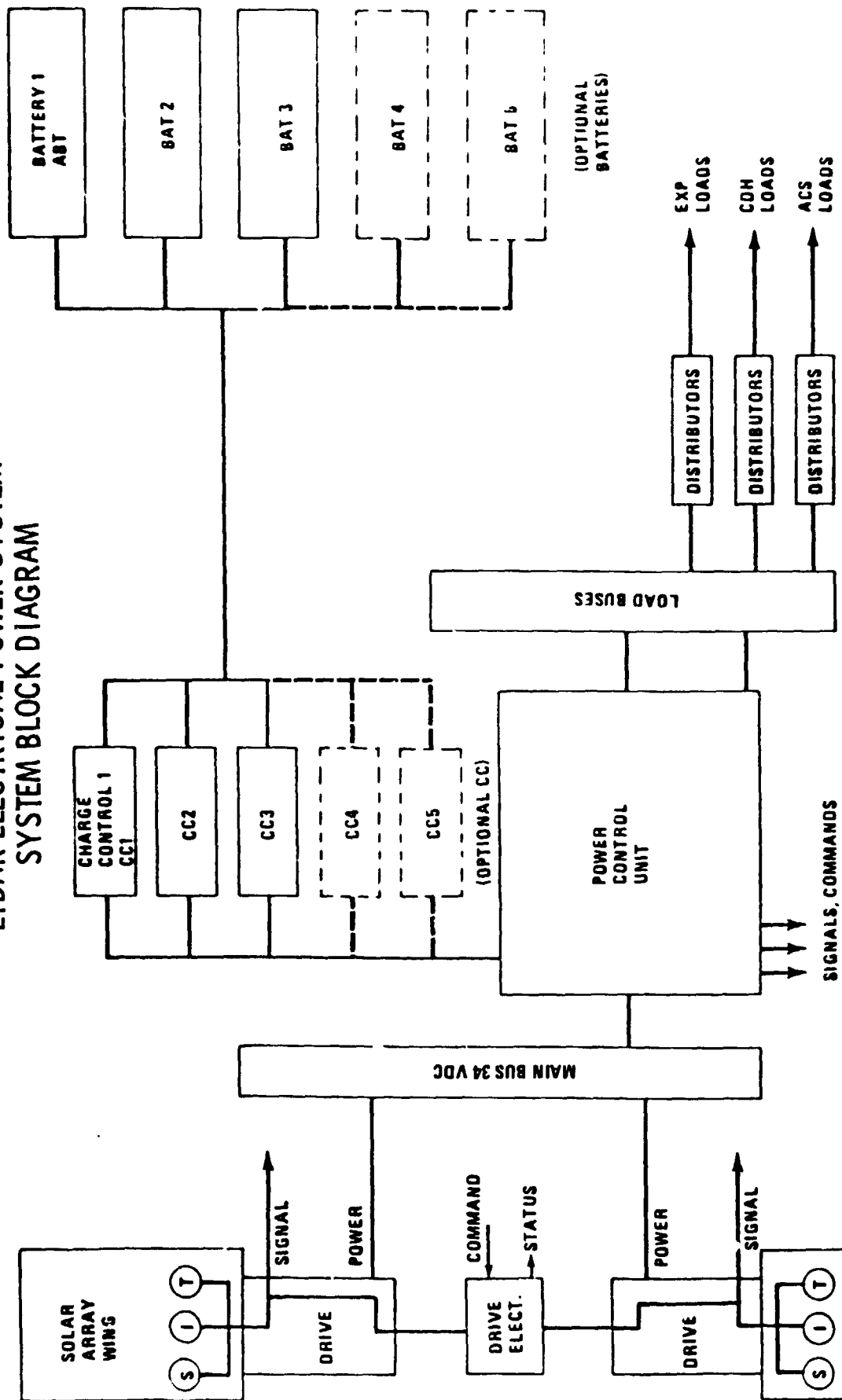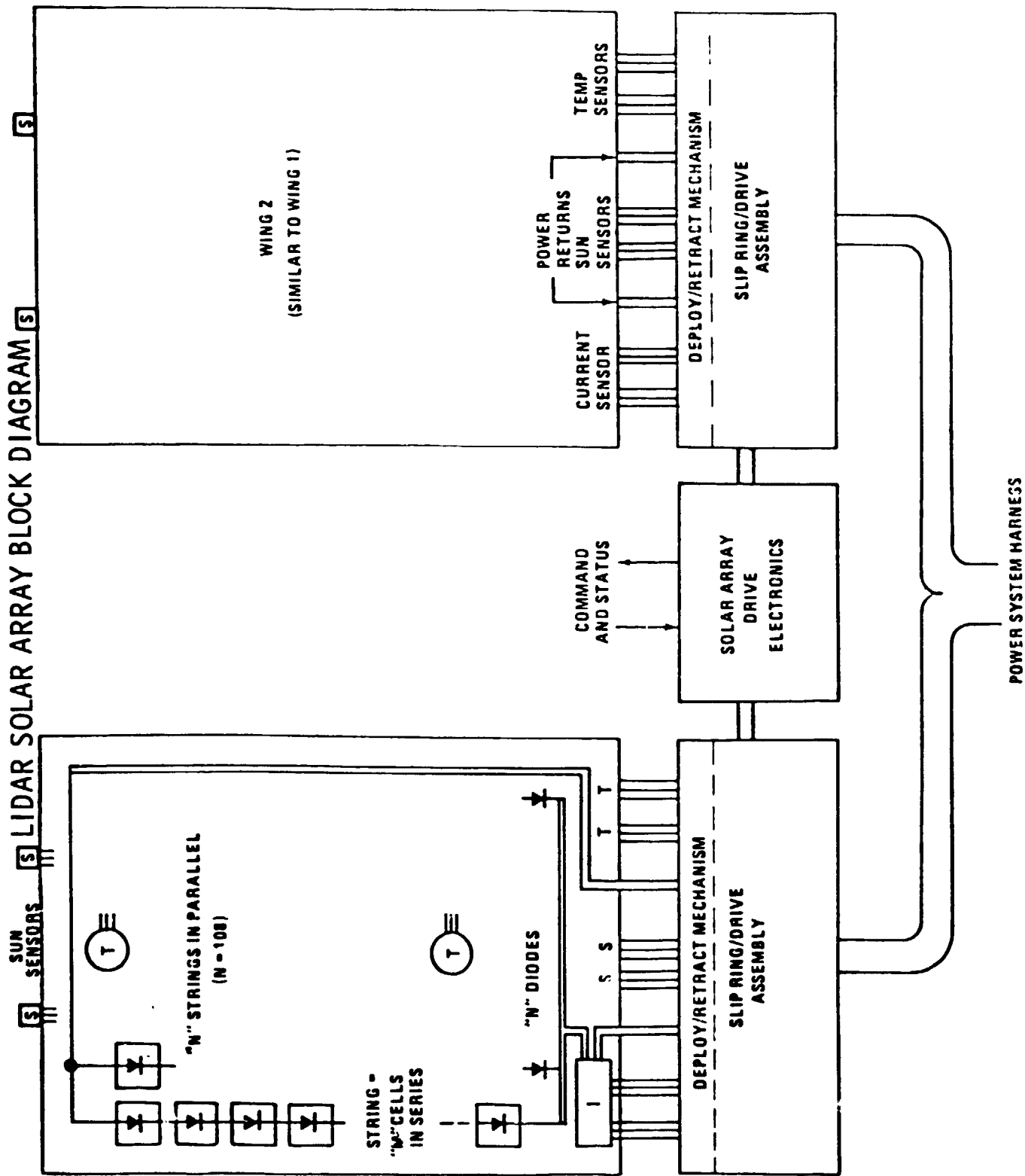LIDAR ELECTRICAL POWER SYSTEM
SYSTEM BLOCK DIAGRAM

33

FIGURE IV. A-2

LIDAR SOLAR ARRAY BLOCK DIAGRAM

energy storage capacity requirement. Apart from relatively standard allowances for conversion and transmission efficiencies, the variation in the suntime fraction during the year must be accounted for. This fraction is shown in figures IV.A-3 and IV.A-4 as "percent time in sun" (PCTIS). For an 800 km, sun-synchronous, orbit with an 0600 hr node, Figure IV.A-3 shows that the spacecraft is continuously in the sun except for a period of about 75 days centered around the summer solstice, when the minimum orbital suntime percent is 83.6%. In contrast, Figure IV.A-4 shows that a spacecraft in an 800 km, 57 deg orbit is occulted on almost every orbital revolution, frequently by as much as 35%. Figure IV.A-5 defines the end-of-life solar array power requirements associated with the candidate orbits.

Figure IV.A-6 shows a cross-section of the solar array, indicating the typical components of a lightweight, rigid honeycomb core type panel. Detailed test data on high-efficiency solar cells (from JPL) were used to select the baseline solar cell and to establish the electrical and thermal operating points (The cell conversion efficiency is sensitive to the cell temperature: at high temperatures, the voltage drops rapidly and, while the current increases slightly, the next effect is decreased output power at the operating point.). Application of estimated degradations due to irradiation and thermal cycle and micrometeorite damage, together with allowances for Earth orbit eccentricity, assembly losses, interconnections, panel layout and accessory components, yields an estimate of the beginning-of-life (BOL) array output requirement. This estimate of the array size also allows estimation of the total wire length/mass connecting the array to the spacecraft. Figure IV.A-7 defines the BOL power requirement for the various orbits considered. Figure IV.A-8 defines the corresponding total EPS masses: the primary differences are due to

(1)   additional battery capacity for increased night times, and

(2)   additional solar array area to charge the extra battery capacity.

IV.B   COMMUNICATIONS AND DATA MANAGEMENT

IV.B.1   DATA RATES

The maximum data rate requirements for the CDMS can be derived straightforwardly by considering the temporal and spectral characteristics of the doppler-shifted pulse backscattered from the atmosphere.

35

FIGURE IV. A-3
SUNTIME FRACTION
(SUN-SYNCHRONOUS ORBIT)

ALTITUDE = 800 KM
INCLINATION = 98.6 DEG
NODE = 0600 HR

TIME FROM VERNAL EQUINOX (HR)
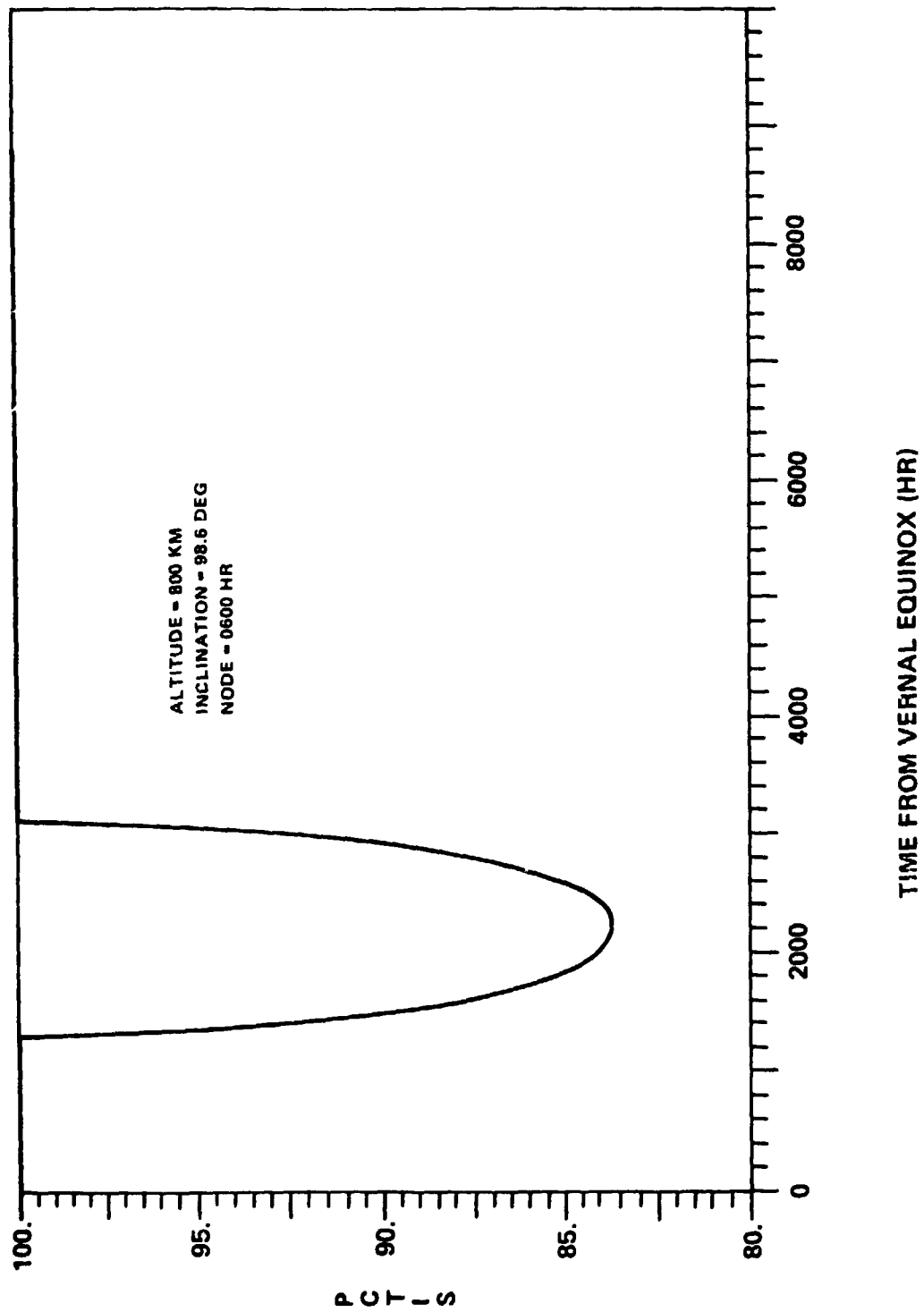
FIGURE IV. A-4
SUNTIME FRACTION

ALTITUDE = 600 KM
INCLINATION = 57 DEG
INITIAL NODE = 060 HR

TIME FROM VERNAL EQUINOX (HR)
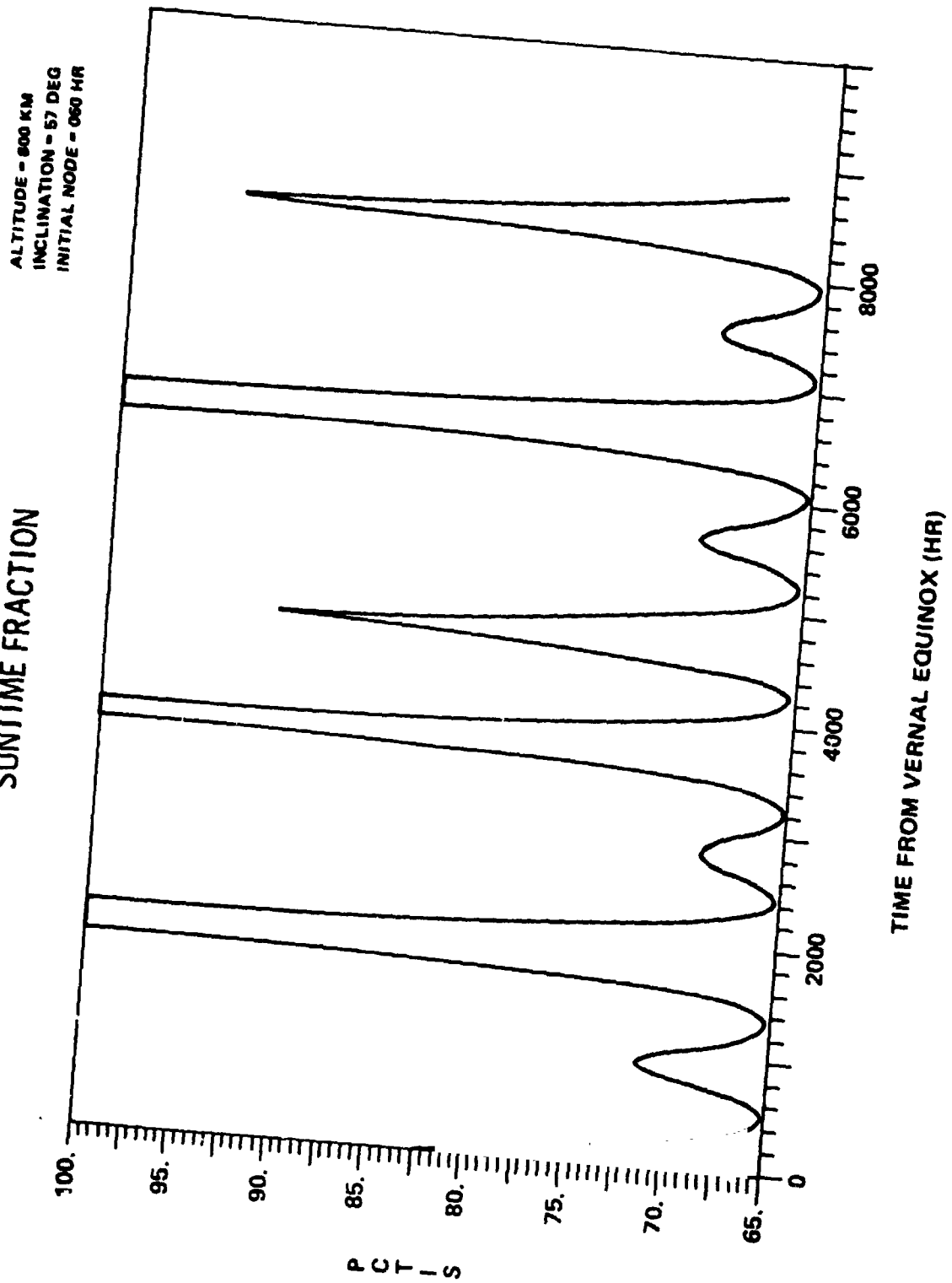
FIGURE IV. A-5
LIDAR ELECTRICAL SYSTEM –
EFFICIENCY BLOCK DIAGRAM
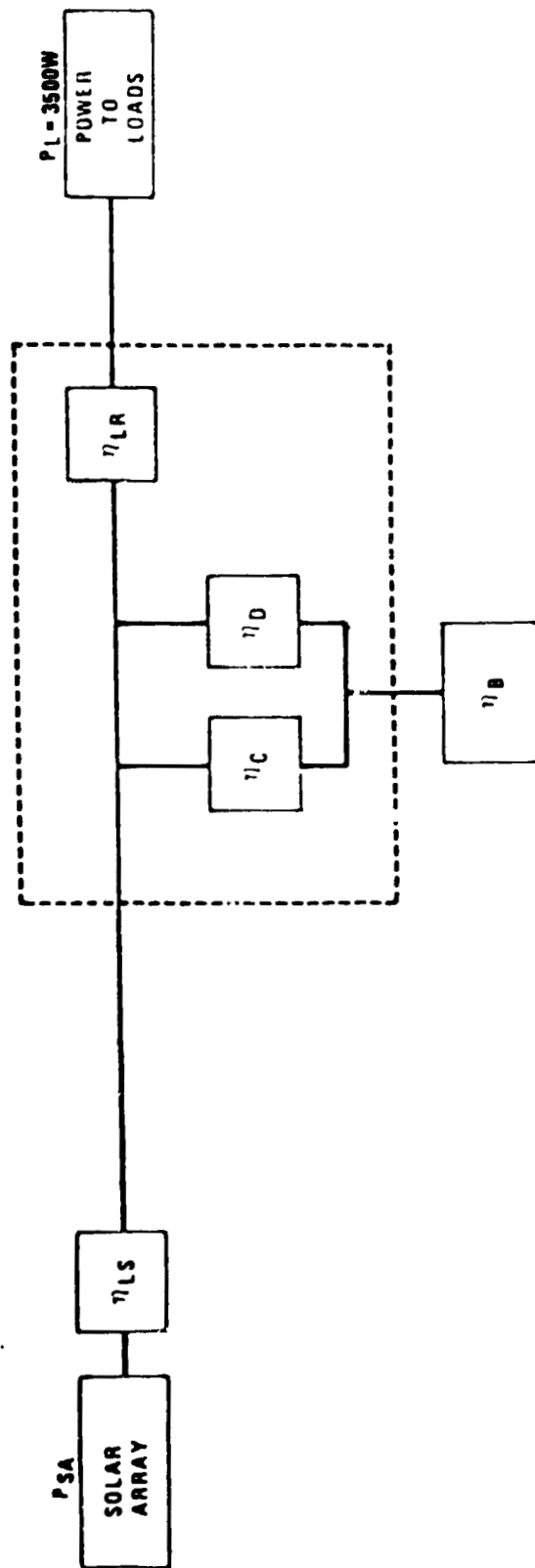
PSA (EOL ARRAY POWER)

	CASE 1	CASE 2	CASE 3	CASE 4	CASE 5	
ALTITUDE	800/8:00	650/6:00	800/12:00	800/57°	500/57°	Km
MAX. NIGHT	992	1143	2105	2087	2145	SEC
MIN. DAY	5058	4718	3945	3963	3529	SEC
PSA	4591	4793	6127	6095	6468	WATTS

2504—81

38

FIGURE IV. A-6
SOLAR ARRAY CROSS SECTION

SOLAR CELL STACK

Layer	Thickness	Weight
COVERSLIDE	.006"	1.015 GRAMS
ADHESIVE	.002"	.195
SOLAR CELL	.002"	.400
ADHESIVE	.002"	.060
		.195
INTERCONNECTIONS		1.865 GRAM/STACK (5CM X 5CM)

SUBSTRATE

Layer	Thickness	Weight
FACE SHEET	.003"	107 GRAM/M^2
ADHESIVE	–	73
CORE	.400"	257
ADHESIVE	–	73
FACE SHEET	.005"	90 } PERFORATED AND COATED
COATING	–	
		600 GRAM/M^2
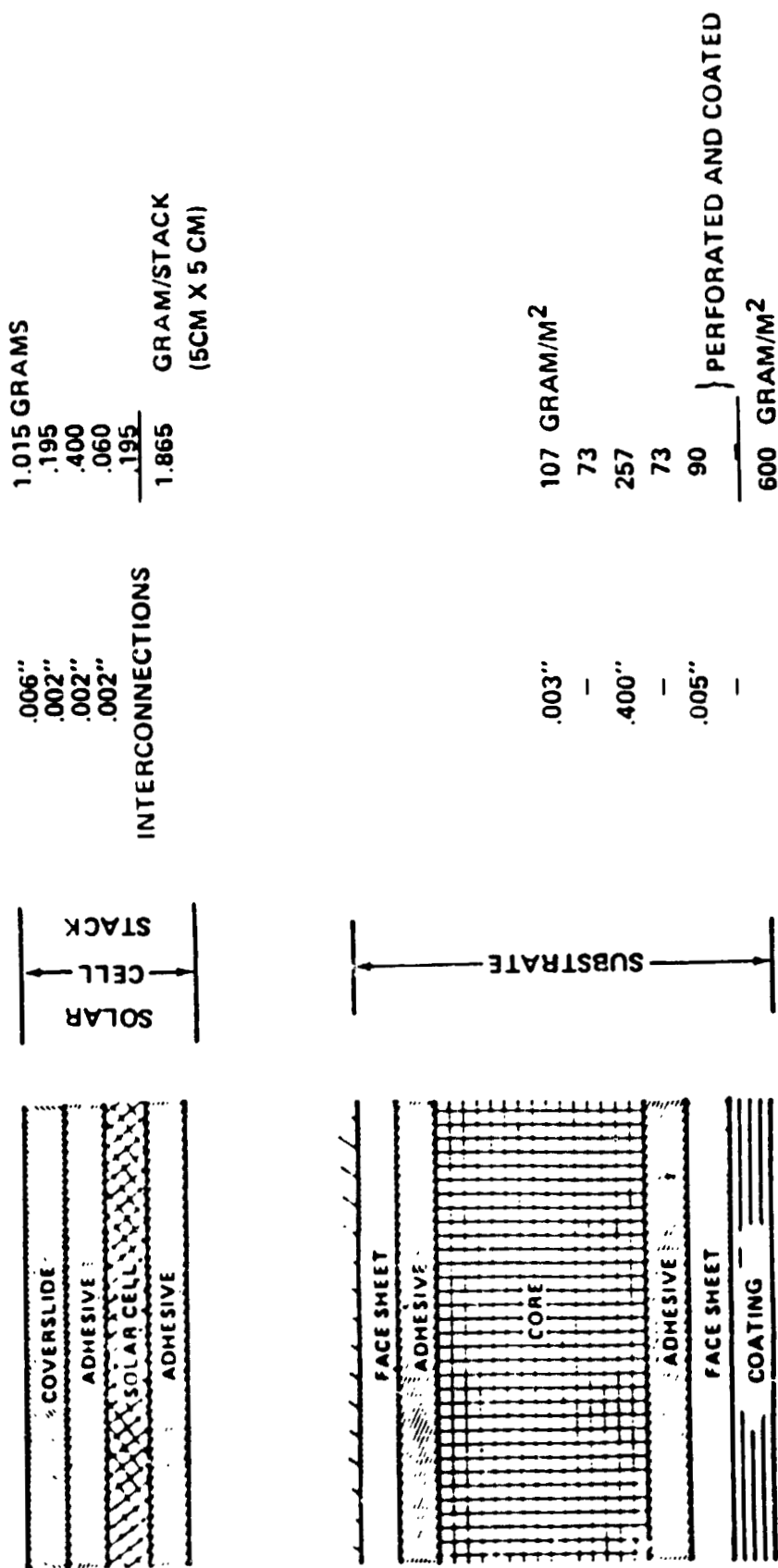
FIGURE IV. A-7
SOLAR ARRAY SIZING

2506-81

SOLAR ARRAY DEGRADATIONS

SOLAR ARRAY RATING

P_{SAR} — N_Q — N_P — N_Q — N_R — N_S — P_{SA} SOLAR ARRAY POWER

APHELION
RADIATION
MICRO METEORITE
U/V, ASSEMBLY
THERMAL CYCLE
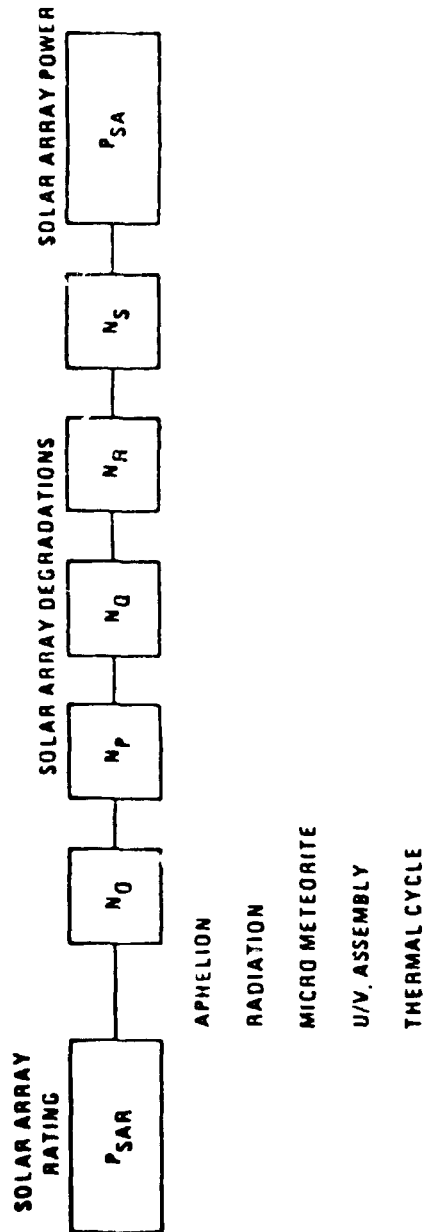
PSAR (BOL ARRAY POWER)*

	CASE 1	CASE 2	CASE 3	CASE 4	CASE 5	
ORBIT	800/6.00	650/6.00	800/12.00	800/57°	500/57°	KM
PSAR	6012	6290	8040	7998	8488	WATTS

*P_{SAR} IS THE BEGINNING OF LIFE (BOL) SOLAR ARRAY POWER OUTPUT
AT OPERATING TEMPERATURE AND ILLUMINATION

40

FIGURE IV. A-8
LIDAR EPS SUMMARY

ORBIT { ALTITUDE (KM) / INCLINATION / NODE (HR) }	800 SUN SYNC 0600	650 SUN SYNC 0600	800 SUN SYNC 1200	800 57 ANY	500 57 ANY
SOLAR ARRAY SUBSYSTEM					
SOLAR ARRAY	115	121	155	154	163
DRIVE/DEPLOYMENT	68	68	80	80	80
DRIVE/DEPLOYMENT ELECT.	18	18	18	18	18
DIODE ASSEMBLY	14	14	18	18	18
SUB TOTAL	215	221	271	270	279
POWER CONTROL & ENERGY STORAGE					
POWER DISTRIBUTION	23	23	23	23	23
POWER CONTROL	45	45	55	55	55
CHARGE CONTROL	7	7	11	11	11
BATTERY	98	98	250	250	250
SUB TOTAL	173	173	339	339	339
POWER DISTRIBUTION					
EQUIPMENT HARNESS	125	125	136	136	136
PAYLOAD HARNESS	68	68	68	68	68
SUB TOTAL	193	193	204	204	204
TOTAL, KG	581	587	814	813	823

41

Figure IV.B-1(a) illustrates the temporal characteristics, using representative numerical values taken from the NOAA/LMSC study final presentation charts. A laser pulse of about 5 μs duration is transmitted from the spacecraft into the atmosphere, from which backscattering occurs until the trailing edge of the emitted pulse reaches the surface. Thus, the duration of the return pulse is

$$2 \frac{AID}{c} + \tau$$

where

AID = Atmospheric Interaction Distance

c = Speed of light

τ = Emitted pulse duration

or about 350 μs for the parameters assumed in the NOAA/LMSC study. This can be chopped into 20 "range bins" of 17.5 μs duration, each corresponding to a 1 km vertical resolution.
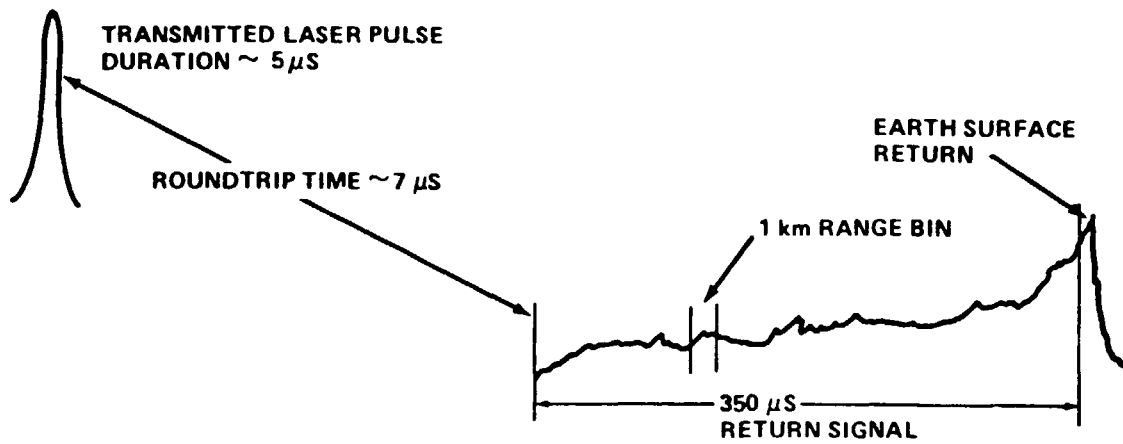
Figure IV.B-1(b) illustrates the essentail spectral characteristics. The greatest frequency shift is due to the spacecraft motion relative to the Earth (about $\pm$ 1.5 GHz, depending on whether the laser "firing direction" is along or against the space craft motion). The doppler shift due to a $\pm$ 1 m/s wind is about 220 kHz - leading to a 44 MHz bandwidth for measuring $\pm$100 m/s winds. The sampling rate is then 88 MHz, or about 100 MHz. Based on the NOAA and LMSC studies, a 4 bit quantization has been selected Thus, each pulse generates 140 kbit of phase information. At 8 pulses every second, this yields 1.12 Mbps of phase data. Quantizing the amplitude data at 10 bits, for each range bin, and at a 1 MHz sample rate, yields an additional 30 kbps.

The total raw data rate is then about 1.15 Mbps. Capability for downlinking this data is necessary, at least initially, for evaluation and special studies. Operationally, such a flood of data is neither necessary nor desirable, and some form of onboard preprocessing must be considered.
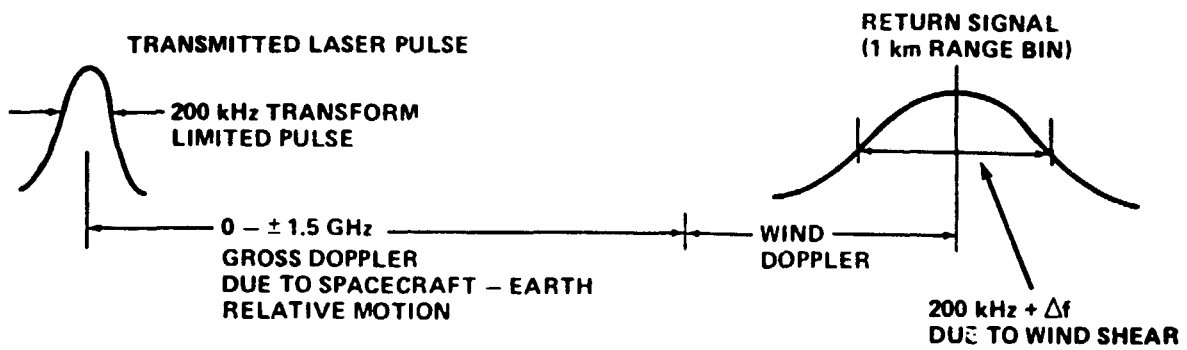
At the extreme, this preprocessing may reduce the data for each range bin to three quantities indicative of the radial component of the wind, the dispersion due to shear and turbulence, and the signal strength. With an austere allowance for data defining the orientation of each "shot" relative to the Earth, 5 Kbps emerges as a lower limit for the preprocessed data downlink rate.

These downlink data rates (raw and preprocessed) could be halved if the number of range bins is halved (either

FIGURE IV. B-1

TRANSMITTED LASER PULSE
DURATION ~ 5 μS

ROUNDTRIP TIME ~ 7 μS

EARTH SURFACE
RETURN

1 km RANGE BIN

←————— 350 μS —————→
RETURN SIGNAL

(a) TEMPORAL CHARACTERISTICS OF LIDAR PULSE

TRANSMITTED LASER PULSE

RETURN SIGNAL
(1 km RANGE BIN)

200 kHz TRANSFORM
LIMITED PULSE

←———— 0 – ± 1.5 GHz ————→|←— WIND ——→
GROSS DOPPLER   DOPPLER
DUE TO SPACECRAFT – EARTH
RELATIVE MOTION

200 kHz + Δf
DUE TO WIND SHEAR

(b) FREQUENCY CHARACTERISTICS OF LIDAR PULSE

by halving the vertical range or increasing the vertical resolution to 2 km). Conversely, if the quantization of phase data were increased from 4 to 8 bits, the downlink rates would be doubled.

IV.B.2. TDRSS UTILIZATION

Figure IV.B-2 illustrates the positioning of the two geostationary TDRSS spacecraft. One consequence of this positioning is the presence of a "dead zone" in which the spacecraft will be out of contact with both TDRSS spacecraft. Figure IV.B-3 depicts the geographic location and extent of this dead zone for a spacecraft with an orbital altitude of 500 km. There are three categories of TDRSS service to be considered:

o   Multiple Access (MA)
         -   Up to 20 users/TDRS
         -   Up to 50 kbps downlink rate

o   S-band Single Access (SSA)
         -   Two user/TDRS
         -   Up to 3 Mbps downlink rate

o   Ku-band Single Access (KuSA)
         -   Two user/TDRS
         -   Up to 300 Mbps downlink rate

The multiple access service would limit the system to transmission of data processed to less than 50 kbps (less, to allow for housekeeping, attitude, and position data). Although the TDRSS operational modes have not been fixed at this time, there is reason to believe that MA channels may not be available to a single user for years of operation. The multiple access service does not provide a useful capability for transmission of unprocessed data.

The SSA service appears to be the preferred service for this application: A limited amount of unprocessed data can be downlinked in real time and processed data can be handled with a store-and-dump mode using NASA standard 10^8 tape recorders. The principal issue relative to the store-and-dump mode is tape recorder life, the main limits on which are the numbers of tape and negator spring reversals (there being two of the latter for each of the former). The recorder is designed for 20,000 tape passes and 50,000 spring reversals. Twenty-eight transports have been flown, and have accumulated 51,000 hours of operation without a major failure. If the maximum recorder dump rate (2.5 Mbps) is used - a parallel track dump - then parallel recording must be used. Figure IV.B-4 describes the relationship between the record rate and the recorder tape/negator spring life limits for two cases: A single recorder and dual recorder
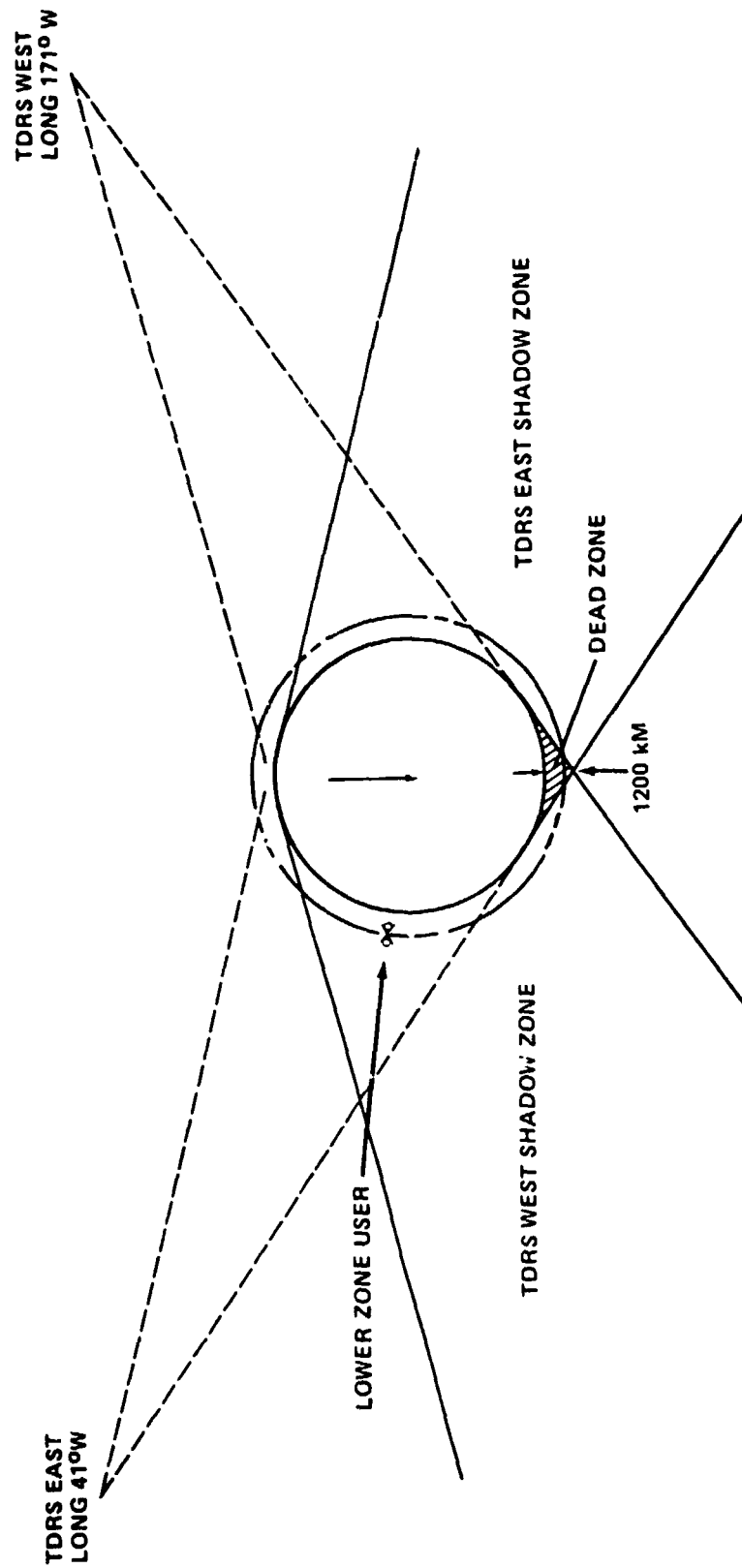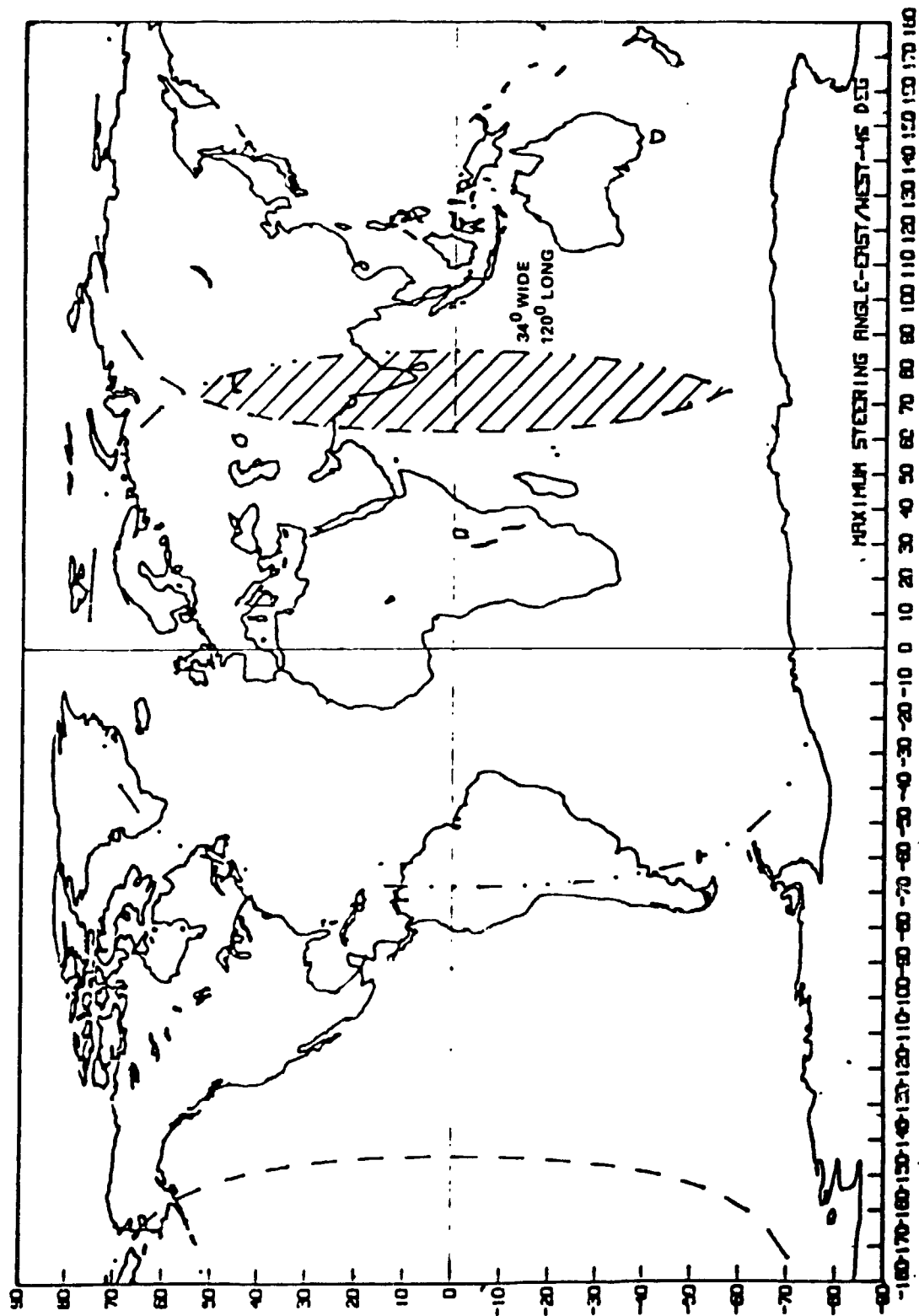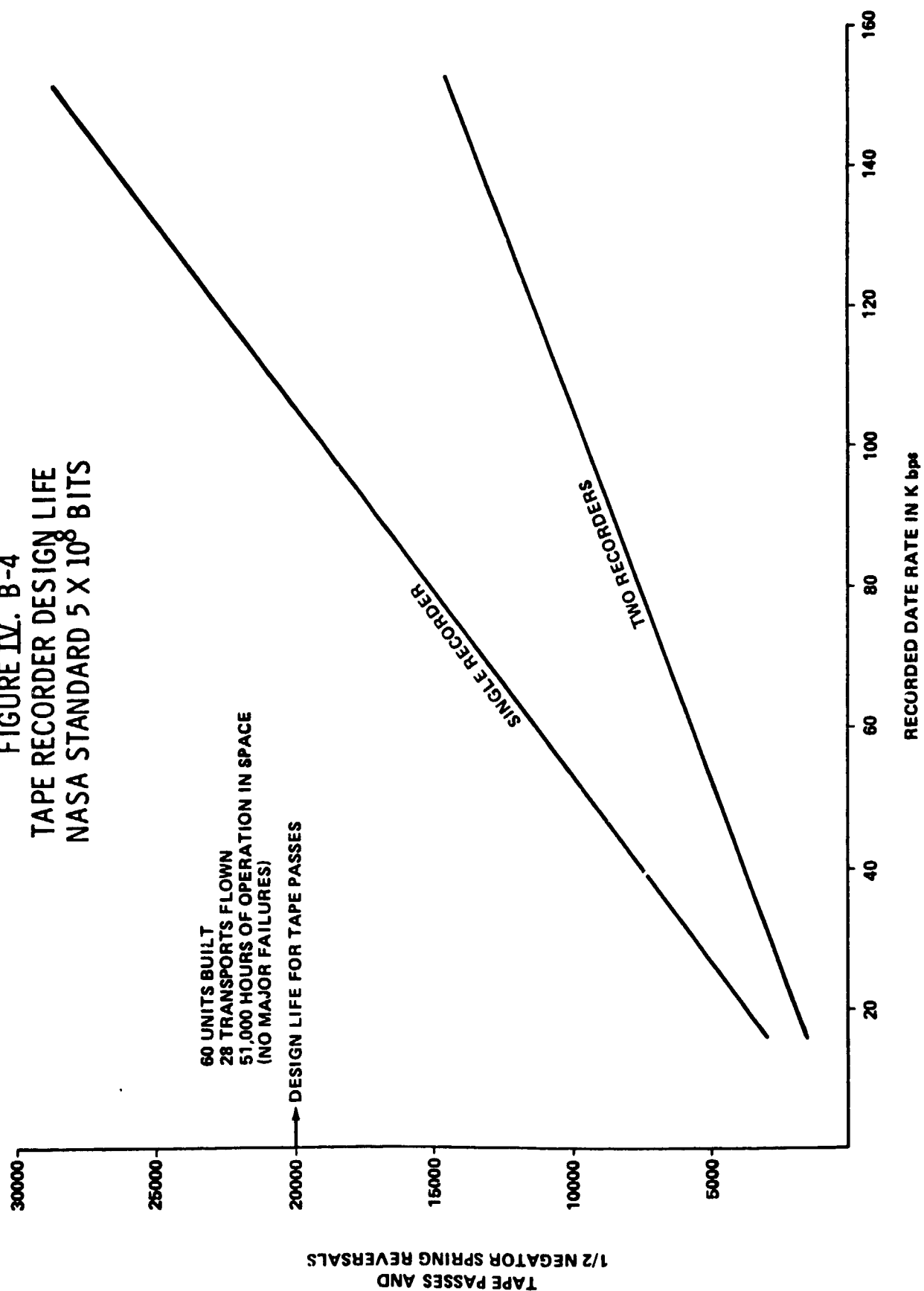
FIGURE IV. B-2
TDRSS COVERAGE GEOMETRY

TDRS WEST
LONG 171° W

TDRS EAST SHADOW ZONE

DEAD ZONE

1200 kM

LOWER ZONE USER

TDRS WEST SHADOW ZONE

TDRS EAST
LONG 41°W

FIGURE Ⅳ. B-3

TDRSS DEAD ZONE, USER ALTITUDE = 500 km

34° WIDE
120° LONG

MAXIMUM STEERING ANGLE-EAST/WEST-45 DEG

FIGURE Ⅳ. B-4
TAPE RECORDER DESIGN LIFE
NASA STANDARD 5 X 10⁸ BITS

60 UNITS BUILT
28 TRANSPORTS FLOWN
51,000 HOURS OF OPERATION IN SPACE
(NO MAJOR FAILURES)
→ DESIGN LIFE FOR TAPE PASSES

47

operated in a flip - flop mode. Limiting the record rate to no more than 50 kbps not only provides a 50% margin on tape passes, but permits an alternate mode usable in the event of tape recorder failure: processed data would be downlinked continuously using MA service to the extent allowed by competing traffic (while not in a dead zone).

The technical requirements of the doppler lidar wind-measuring system are satisfied by the SSA service: this is also the most economical approach, based on the current "soft" TDRSS use charges (the charge rates used are not official but are accepted figures for planning purposes). For the MA service, assuming continuous telemetry of data processed to less than 50 kbps, the three-year mission use charge would come to $6.57 M. In contrast, the corresponding use charge for SSA with a store-and-dump mode at a 50 kbps record rate / 2.5 Mbps dump rate is $2.63 M. The S-band communication equipment is the same in either case, and three NASA standard recorders at approximately $500 K each are required for the SSA mode (two to ensure no loss of data, and an additional recorder to allow one failure without degradation of system performance). The SSA use charge may be significantly lower if the recorders can be dumped to exploit the TDRSS "as available" rates.

No need for downlinking large quantities of unprocessed data have been identified: if such a need does arise, a store-and-dump mode utilizing the KuSA service will need to be considered. The limiting factor in this instance will be the tape recorder dump rate. The Spacelab High Data Rate Recorder (HDRR) could be used; its maximum dump rate of 32 Mbps would result in a KuSA utilization rate of about 7%. At a charge of $5,000/hr, the resulting use charge for a three-year mission is $9.2 M. The cost of the Ku-band communications equipment and adaptation of the HDRRs would likely equal or exceed this figure.

IV.B.3.   CDMS CONCEPT

Figure IV.B-5 illustrates the basic CDMS concept for the doppler lidar wind measuring spacecraft. Since a nominal 3-years mission is appropriate for a free-flying spacecraft, redundant hardware has been provided. The A/D converters and the preprocessor are "special purpose" items and will probably not be considered a part of the CDMS.

For routine operations, the preprocessor reduces the 1.15 Mbps stream of amplitude and phase data to a rate between 14 and 48 kbps; this preprocessed data is multiplexed with telescope and spacecraft navigation and housekeeping data to form a stream of no more than 50 kbps. This final stream is either recorded for later playback or downlinked

FIGURE IV B-5
DOPPLER LIDAR SPACECRAFT
COMMUNICATION AND DATA MANAGEMENT BLOCK DIAGRAM
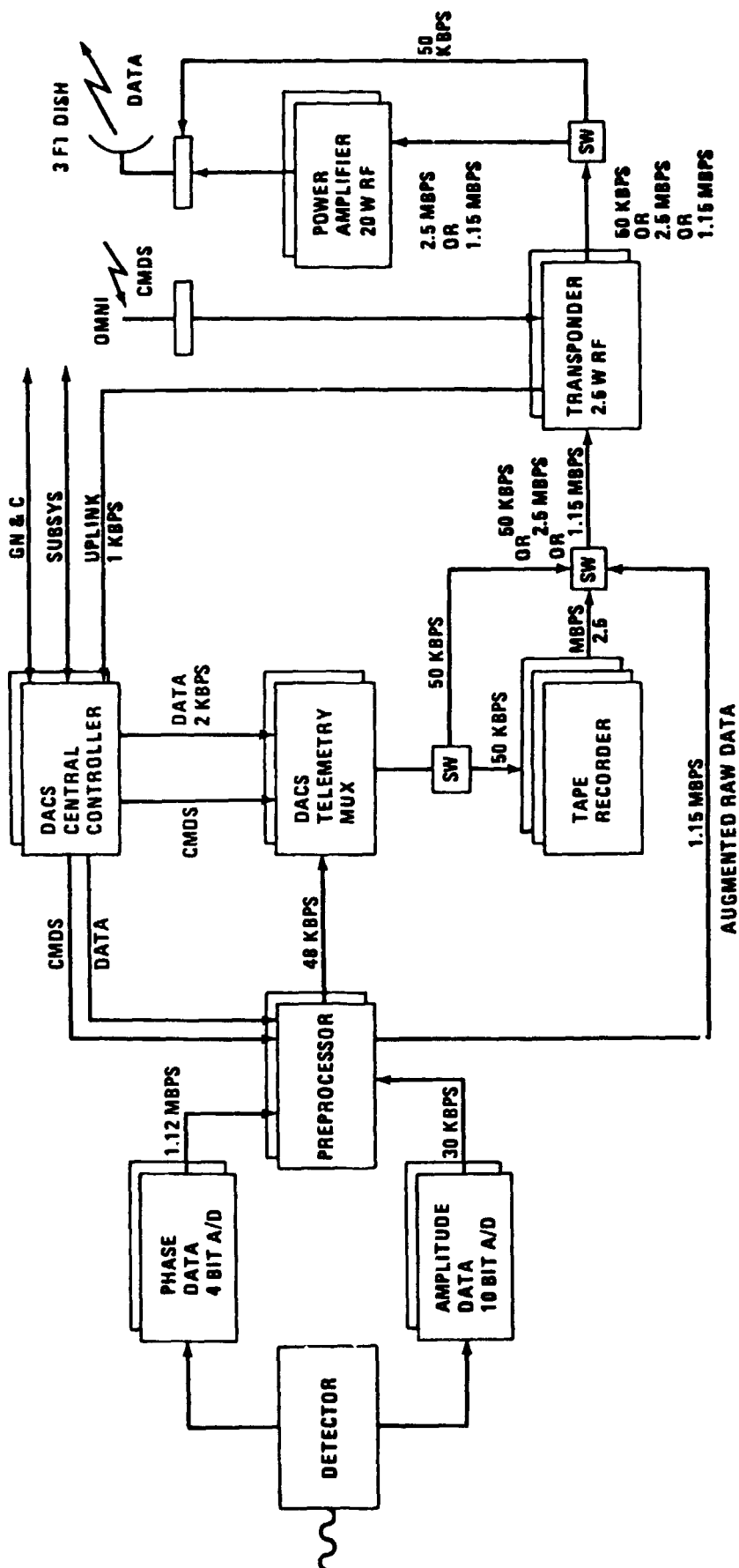
through the TDRSS MA channel. The MA service utilization capability is intended to satisfy currently unanticipated needs and to provide a means of circumventing tape recorder problems/failures. Normally, a full recorder is dumped at 2.5 Mbps while another is recording. One of the recorders can fail with no effect. After the second recorder failure, no data can be recorded while the survivor is in the dump mode - about 2% of the time if data is recorded at 50 kbps.

A secondary mode routes unprocessed amplitude and phase data, augmented by telescope and spacecraft navigation data, through the TDRSS SSA in near-real-time. Such data would not be transmitted while in the TDRSS dead zone. In this mode, the preprocessor also acts as a multiplexer.

Figure IV.B-6 is the equipment list for the CDMS. The totals for mass and power, conservatively estimated, are 68 kg and 187 watts. If a mission profile were run, the total power to support the CDMS would be less. For instance, one transponder was considered to be on and transmitting at all times, which would not be the case for a store-and-dump mode. The conservatism should have little effect on the overall spacecraft, as the CDMS power requirement is less than 10% of the power needed for the mission equipment.

IV.C.   ATTITUDE CONTROL AND DETERMINATION

IV.C.1.   ATTITUDE CONTROL REQUIREMENTS

Two distinct sets of attitude control requirements flow from the mission objectives.

For large-area wind estimation, the telescope scanning mechanism provide one element of beam pointing; the attitude control functions are then to

> o   align the telescope scan axis (nominally the spacecraft z-axis) with the local vertical (The spacecraft coordinate system is illustrated in Figure IV.C-1) and

> o   roll the spacecraft about the z-axis to orient the radiators and solar arrays.

Radiator and solar array orientation is relatively undemanding: with the spacecraft z-axis aligned with the local vertical, the spacecraft is rolled until the sun is in the plane of the radiators (i.e., the yz-plane). Normally prudent design practice will oversize the radiators to allow 1-3 degrees of misorientation (in any axis). This roll

50

FIGURE IV. B-6
CDMS SUMMARY

| ITEM	NUMBER REQUIRED	UNIT SIZE (CM)	UNIT MASS (kg)	UNIT POWER (W) OPERATIONAL/STANDBY
1. A/D CONVERTER	4	10 X 15 X 5	1.0	5/1
2. PREPROCESSOR	2	30.5 X 25.5 X 7.5	6.0	25/10
3. DATA ACQUISITION & COMMUNICATION SYSTEM (DACS)	4	20 X 18 X 11	3.2	13/4
4. TAPE RECORDER	3	15 X 20 X 20	6.4	8W (RECORD) 17W (PLAYBACK) 2W (STANDBY)
5. TRANSPONDER	2	20 X 21 X 9	3.0	10/5
6. TDRSS DISH ANTENNA	1	91 DIA. X 15	10.0	*
7. OMNI WHIP ANTENNA	2	30	1.0	*
8. POWER AMPLIFIER	2	11.5 X 6.5 X 2	0.9	60/10

FIGURE IV. C-1 SPACECRAFT COORDINATE SYSTEM
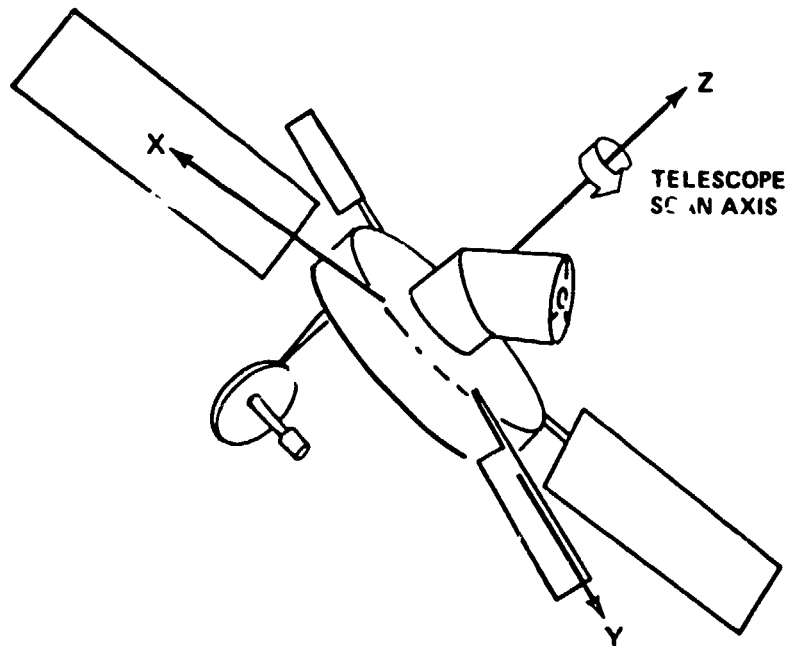
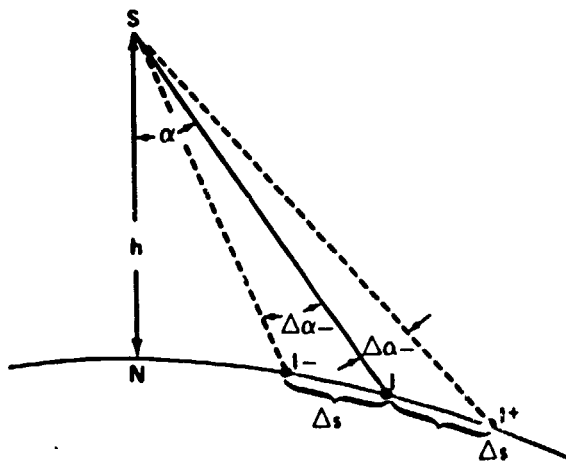# FIGURE IV. C-2
LOCAL VERTICAL MISALIGNMENT GEOMETRY

S: SPACECRAFT POSITION

N: NADIR POINT

h: SPACECRAFT ALTITUDE

α: SCAN ANGLE

I: PULSE IMPACT POINT WITH NO
    LOCAL VERTICAL MISALIGNMENT ERROR

ΔS: ALLOWABLE MISS DISTANCE

I$\pm$: PULSE IMPACT POINTS ON GREAT
    CIRCLE NI HAVING MISS DISTANCES ΔS

$\Delta\alpha\pm$: ASSOCIATED LOCAL VERTICAL
    MISALIGNMENT ERROR

maneuver also orients the solar arrays: the rotational capability (beta-angle compensating) provided for these will then maximize the output power. Again, a misorientation of 1-3 degrees will have no significant effect.

No firm requirement for the alignment error of the z-axis and local vertical has been derived from the large area wind measurement objective. Obviously, the error should not be so great that some of the lidar pulses miss the Earth entirely. This consideration leads to an upper bound of 5-10 degrees for the allowable error. A tighter bound will be necessary, for the return signal from pulses which reach the horizon will have too low a signal-to-noise ratio to be useful (at least at the lower altitudes).

A tentative criterion for the alignment error can be based on the observation that the reference pulse rate and scan rate imply an "average" Earth surface sample area of about 50 km x 50 km. This suggests that each pulse should strike the surface within 25 km of the point it would strike if there were no error. Figure IV.C-2 illustrates the geometry. If the allowable miss distance is 25 km, the corresponding allowable angular misalignment is 5 mrad at a spacecraft altitude of 800 km, 3.9 mrad at 550 km. A constant, or slowly varying, error of this magnitude may not be important, depending on the orientation of the error. For example, referring to Figure IV.C-2, suppose the spacecraft velocity vector is in the plane of the paper, directed to the right. The error then lies in the orbital plane, and the effect is to shift the scan pattern forward or backward along the ground track. On the other hand, suppose the velocity vector is perpendicular to the plane of the paper. The error is now normal to the orbital plane, and the effect is to shift the ground track left or right. The effect of the pattern shift of this magnitude along the ground track poses no problems in itself; the same is true of a crosstrack shift so long as no large coverage gaps are introduced. The overlapping of coverage swaths away from the equator suggests that a constant or slowly -varying crosstrack local vertical alignment error of 4-10 mrad is tolerable.

A further tightening of the local vertical alignment error requirement may arise from consideration of the lag angle miscompensation resulting from the error. This miscompensation will likely be dependent on the design of the lag angle compensator/beam steering subsystem. In any event, the resulting error will reduce the SNR of the return.

As noted in Section I.C., the requirements for the second mission objective (i.e., a capability for intensive local observation) are poorly defined at this point, with ground truthing and localized meterological phenomena being the obvious considerations. The technique currently

envisioned for realizing this objective entails halting the telescope scan, locking the telescope, discontinuing lag angle compensation, and pointing the telescope axis at an atmospheric targic by using the attitude control system. The definition of the 10 km horizontal resolution (i.e., 10 km x 10 km surface-level target) mentioned in the WPL-37 and -63 reports seems to have been chosen with "ground truthing" in mind: such a target might be reasonably studied by ground-based, balloon-, and aircraft-borne sensors, and the results compared to observations from space.

There are some obvious p:ints to be considered in connection with localized observations. If the atmospheric volume to be observed is small (a few tens of kilometers) and located in the orbital plane, the crosstrack component of the wind cannot be measured reliably. If the volume is not in the orbital plane, and the angle between the local vertical from the spacecraft and the spacecraft-to-target line-of-sight is greater than the operational scan angle, then the SNR will be reduced, with accompanying reduction in wind measuring accuracy. Also, a given small atmosphere target will not be viewable "on demand": if located at the equator, as much as twelve hours could elapse between viewing opportunities (assuming a single spacecraft).

To avoid having this secondary mission objective become a design driver, further definition of observational needs is required, particularly considering the potential for ground truthing by inference.

The WPL-37 report discusses a pointing jitter requirement of 2 μrad/5 msec - which would permit efficient heterodyning, by ensuring overlap of the transmitter and receiver fields of view. The 5 msec here is intended to be representative of the pulse roundtrip time, and the 2 μrad is to include errors due to structural vibrations, lag--angle miscompensation, and scan mirror jitter. Although a requirement of this order is considered achievable, the detailed structural analysis needed for verification is beyond the scope of this assessment activity.

IV.C.2.   ATTITUDE DETERMINATION REQUIREMENTS

Knowledge of spacecraft attitude and position is required for control purposes (e.g., to calculate the orientation of the local vertical in spacecraft coordinates), for gross doppler removal via the frequency synthesizer, and for vector resolution of the horizontal wind. The allowable uncertainty in local vertical alignment corresponding to a horizontal wind uncertainty ΔW is given by the approximation

54

$$E = \frac{\Delta W}{V_c} \tan \alpha$$

where V_c is he orbital velocity and α is the scan angle. For $\Delta W = 1$ m/s and atmospheric coverage at 550 km altitude, $E \approx 220$ μrad. At 800 km altitude, $E \approx 300$ μrad.

The gross doppler induced by spacecraft - Earth motion will also depend on the beam azimuth relative to the spacecraft velocity vector, according to

$$D = \frac{2 V_c}{\lambda} \cos \phi$$

whence

$$\Delta D = \frac{2 V_c}{\lambda} \Delta \phi$$

for $\phi = 90^\circ$ - i.e., the sensitivity to the gross doppler error is greatest when the firing direction is at right angle to the ground track. At 800 km altitude, the uncertainty $\Delta \phi$ corresponding to a 220 kHz doppler uncertainty (1 m/s wind) is 130 μrad.

IV.C.3. ACDS CONCEPT

Figure IV.C-3 illustrates the concept. A system of biased reaction wheels is used to cancel the momenteum of the rotating telescope, and the resulting zero-momenteum system rotates inertially once per orbit to maintain the telescope scan axis along the local vertical. The reaction wheels also provide the torques to control attitude excursions. The magnetic torquers react against the Earth's magnetic field for momenteum desaturation of the wheels. This field can be sensed by the magnetometers, or calculated. The sun sensor is used to define the relationship of the radiators to the sun.

Two-axis star trackers placed on the anti-sun of the spacecraft permit frequent updating of the DRIRU-II reference gyro assembly which serves as the primary attitude reference. The attitude information is combined in the digital processor assembly (DPA) with position and velocity information derived from the global positioning system (GPS) to calculate the orientation of the local vertical in spacecraft coordinates. The DPA then issues commands to the reaction wheels to align the spacecraft scan axis with the local vertical.

Figure IV.C-4 defines the ACDS mass and power requirements.

FIGURE IV. C-3
ATTITUDE CONTROL AND DETERMINATION
BLOCK DIAGRAM
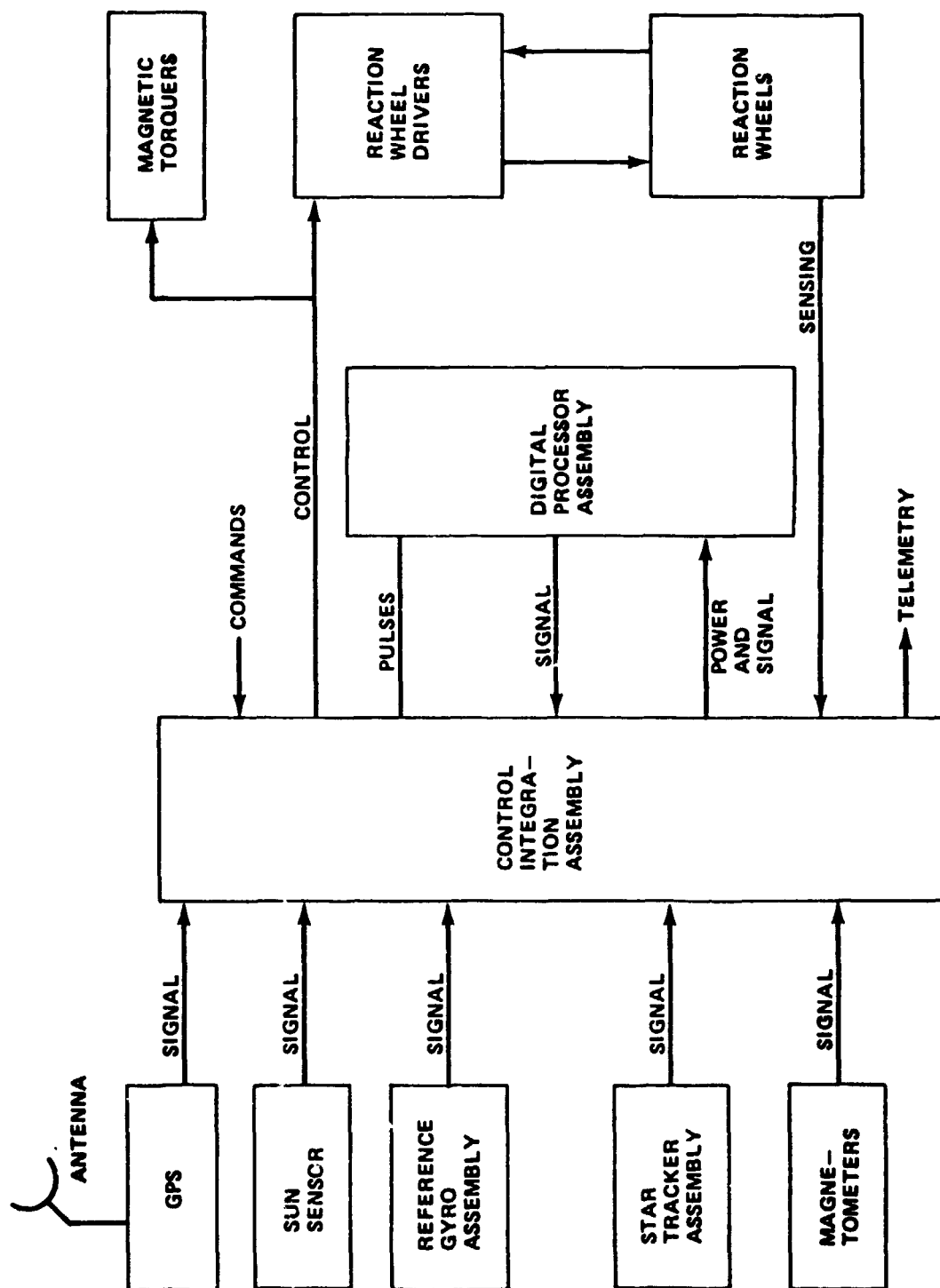
FIGURE IV. C-4
ATTITUDE AND POSITION DETERMINATION
SUMMARY

	NO. REQUIRED	SIZE (CM)	WEIGHT (KG)	POWER (W)
SENSORS				
— STAR SENSOR	2	17.8 X 19.1 X 40.6	9.1	22
— SUN SHADE	2	—	2.3	
— SUN SENSOR	2	—		
— GYRO PACKAGE	1	30.5 X 30.5 X 22.9	15.9	21
— GPS	1	30.5 X 30.5 X 30.5	16.8	20–40
— GPS ANTENNAS	2	20.1 ACROSS	2.0	
— MAGNETOMETERS	2	—	3.0	
CONTROLLERS				
— REACTION WHEELS	4	35.6 DIA X 20.3	15.9	25
— MAG TORQUERS	3	2.5 DIA X 100.1	5.9	2
PROCESSOR	1	24.1 X 24.1 X 26.7	9.1	36

V.   MISSION OPERATIONS AND PERFORMANCE

V. MISSION OPERATIONS AND PERFORMANCE

V.A WIND ACCURACY REQUIREMENT: ORBIT SELECTION

Consideration of WPL-37 and -63 yields the following conclusions:

o   The sensitivity of achievable wind accuracy to orbital altitude and inclination has not been established.

o   This sensitivity is dependent, probably in a vital manner, on atmospheric attenuation and backscatter.

Additionally, whereas prior analyses have consistently considered an 800 km, high-inclination operational orbit

o   Simplified analyses indicate that lower orbital altitudes and inclinations may be possible without important degradation of wind measurement accuracy; some enhancement may be possible.

o   Future trade studies of orbital altitude and inclination versus wind accuracy should be based on simulations of the type described in the WPL reports. Even with such an approach, definite conclusions may be difficult to achieve, due to the uncertainties introduced by imperfectly understood atmospheric phenomena, particularly backscatter.

The remainder of this section interprets wind accuracy as a system figure of merit and traces its (conceptually straightforward) relationship to orbital altitude and inclination. Also, a sun-synchronous and a 57 degree orbital inclination are compared, using various simplifications.

The primary function of the proposed doppler lidar wind measuring system is that of estimating the mean (= average) wind in an atmospheric volume called a resolution element - typically, a horizontal "slab" 1 km deep and 100-500 km on a side. This is done by calculating a (suitably weighted) average of the estimates from a number of pulses (shots) directed into the resolution element from different points along the orbit. From theory, the error in the estimate of the average should decrease as the number of shots is increased, i.e.,

$$\sigma_{avg} \propto \frac{\sigma}{\sqrt{N}}$$

where

σ_{avg} = standard deviation of the wind estimate (m/s)

σ = standard deviation of the estimate of a single shot (m/s)

N = number of shots

The wind accuracy requirement is then expressed as a required value of σ_{avg}. There are two approaches to satisfying the requirement: increase the number of shots, or decrease σ. The improvement by the first approach must ultimately reach a practical limit, imposed by the available power: note that halving the error σ_{avg} requires a quadrupling of the number of shots, and this translates directly into a quadrupling of power.

To understand what is involved in decreasing σ, consider in its place a typical formula for the standard deviation of the radial wind estimate:

where
$$\sigma_r = \left[\frac{\lambda \sigma_v}{2\tau} \left(\frac{1}{4\sqrt{\pi}} + \frac{2\rho}{SNR_w} + \frac{1}{8\pi^2 \rho \, SNR_w^2} \right) \right]^{1/2}$$

λ = doppler-shifted laser wavelength (m)

σ_v = rms velocity width of received spectrum (m/s)

τ = pulse duration (s)

ρ = $\sigma_v / 2\, V_{max}$ where

V_{max} = maximum velocity to be measured (m/s)

SNR_w = wideband signal-to-noise ratio = $\sqrt{2\pi}\, \rho$ SNR

Figure V.A-1, taken from the WPL-63 report, illustrates the variation in the pulse-derived wind accuracy, σ_r , as a function of the signal-to-noise ratio. Figure V.A-2, also taken from WPL-63, carries this one step further, and suggests that the wind measurement accuracy is relatively insensitive to the SNR. However (and as noted), this insensitivity depends upon a number of assumptions, particularly the backscatter profile: the predicted insensitivity is therefore suspect.

If the atmosphere is assumed to be a homogeneous shell of 20 km depth, with an attenuation coefficient of .002 m^{-1} and a backscatter coefficient β = 3 x 10^{-8} $m^{-1}.sr^{-1}$, a simplified SNR expression is
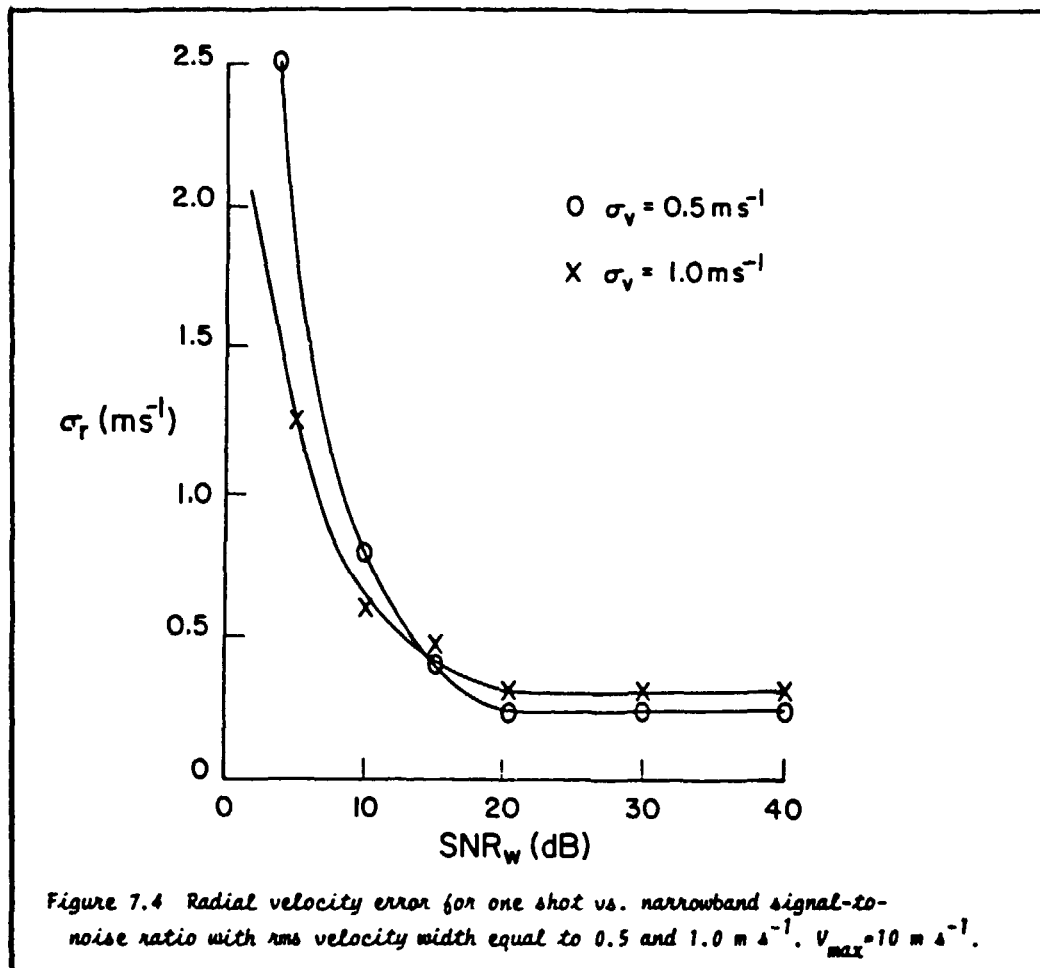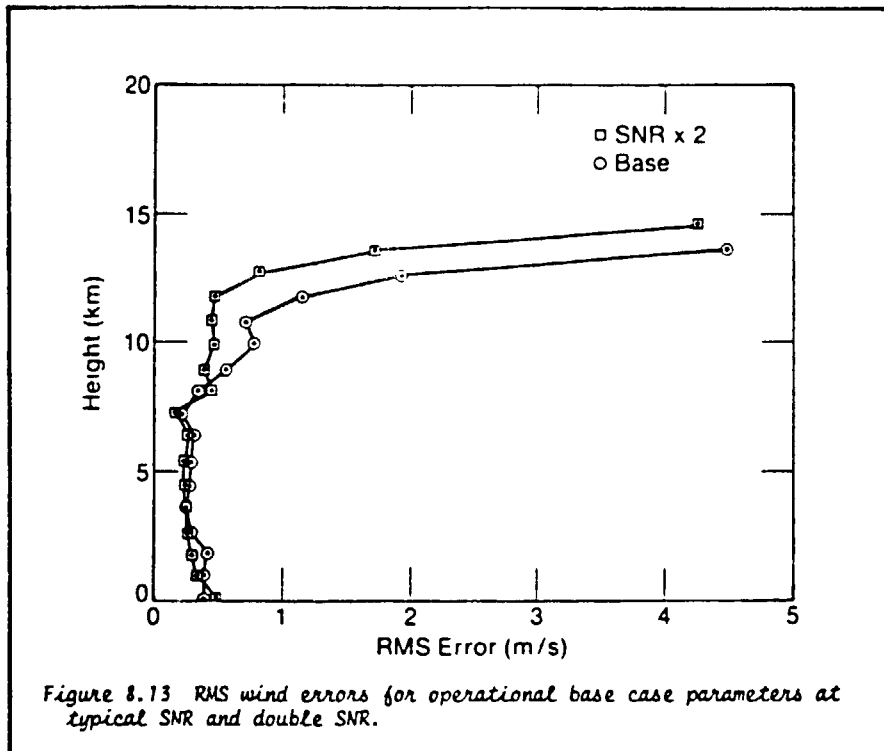
FIGURE V. A-1
WIND ACCURACY VARIATION WITH SNR

Figure 7.4 Radial velocity error for one shot vs. narrowband signal-to-noise ratio with rms velocity width equal to 0.5 and 1.0 m s^{-1}. V_{max} = 10 m s^{-1}.

FIGURE $\underline{V}$. A-2
WIND ACCURACY SENSITIVITY TO SIGNAL-TO-NOISE RATIO

Figure 8.13 RMS wind errors for operational base case parameters at typical SNR and double SNR.

$$SNR= \left[\frac{J\lambda\tau}{\hbar} \right] \left[\beta e^{-2\mu \cdot AID} \right] \left[\eta \frac{D^2}{TSR^2} \right]$$

where

> AID = Atmospheric interaction distance, i.e., distance from ground to top of the atmosphere, along the beam

> TSR = total slant range, i.e., distance from ground to spacecraft, along the beam

Figure V.A-3 displays two sets of SNR curves, one set corresponding to a sun-synchronous orbital inclination; the other, corresponding to a 57 degree inclination. In both cases, the SNR was calculated for the return from the bottom kilometer of the atmosphere, the scan angle was selected to provide contiguous swaths at a height of 20 km at the equator, and the attenuation coefficient was varied by ± 50% to indicate sensitivity.

The first conclusion to be drawn from Figure V.A-3 is that there is an optimum orbital altitude lying between 400 and 600 km. In fact, while an optimum altitude does exist, more detailed calculations accounting for altitude-varying attenuation and backscatter suggest that the optimum may lie above 800 km. However, the variation of the SNR with altitude in the range 500-800 km appears to be less than 3 db, according to these more refined calculations.

The second obvious conclusion is that the SNR is about 2 db greater at the 57 degree inclination than at the sun-synchronous inclination. This has so far been borne out by the more detailed calculations. More extensive and detailed analyses are needed for confirmation; these must carry the SNR results on into the wind accuracy calculation, and account for the various model atmospheres.

V.B.   SHUTTLE PERFORMANCE: DESIGN AND OPERATIONAL
          IMPLICATIONS

Straightforward use of the Shuttle requires placing the doppler lidar wind-measuring spacecraft into its operational orbit and revisiting the spacecraft for retrieval or for servicing and orbital reboost. No other launch vehicle is likely to be available. The basic Shuttle capabilities are inadequate for the orbital altitudes and inclinations of interest (inclination   57 deg, altitude   500 km).The possibilities for achieving these orbits are

o   OMS kits

o   Shuttle augmentation

FIGURE Ⅴ A-3
COMPARISON OF ORBITAL ALTITUDES AND INCLINATIONS
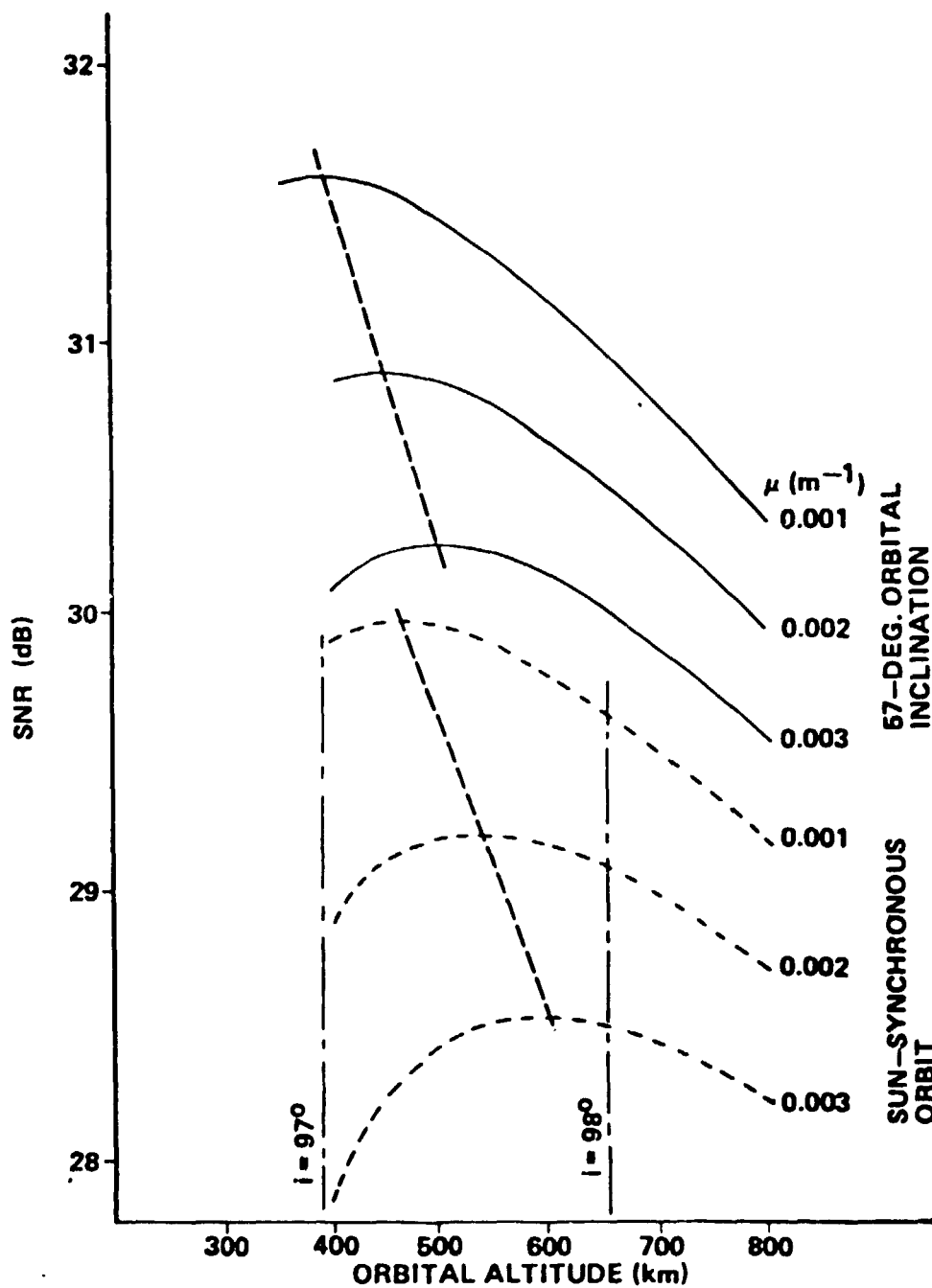
o   Future upper stages

o   Integral propulsion

Figure V.B-1 describes the current Shuttle performance capabilities (JSC 07700, Vol. XIV, Rev. G) for a VAFB launch to a 98 deg-inclination. Even with OMS kits the performance capability is quite limited. Shuttle augmentation provides some relief: Figure V.B-2 is one (unofficial) projection of augmented Shuttle performance capabilities. Even with augmentation, OMS kits are required, and the maximum achievable altitude is only about 680 km.

The current official Shuttle performance projection for a KSC launch does not address inclinations other than 28 deg. Thus, an earlier (again, unofficial) performance projection, given by Figure V.B-3, was consulted. With this projection, the operational spacecraft can be delivered (using OMS kits) to a 57 deg orbit, to an altitude in excess of 800 km, with a considerable performance margin.

Since the Shuttle/OMS kits capabilities to a 57 degree orbital inclination permit a simpler spacecraft design, this should be considered a desirable inclination, subject to coverage and accuracy considerations. The results of this assessment indicate a minor, perhaps even favorable, accuracy effect, as compared to the 800 km orbit considered by NOAA/WPL. Coverage necessarily suffers: with a scan angle selected for a vertical range of 20 km, there is no coverage within about 22 deg of either pole. The impact of this loss of coverage on global prediction models has not been assessed.

FIGURE V. B-1
NEAR TERM CARGO WEIGHT VERSUS CIRCULAR
ORBITAL ALTITUDE-VAFB LAUNCH, DELIVERY ONLY

- SHUTTLE PERFORMANCE IS A FUNCTION OF PROGRAM VARIABLES (LAUNCH DATE, ENGINE THRUST, INDIVIDUAL ORBITER WEIGHT, ETC) AND MUST BE DETERMINED ON A CASE BY CASE BASIS

- CARGO WEIGHT INCLUDES ALL PAYLOAD ITEMS AND PAYLOAD SUPPORT SERVICES

- DATA SHOWN FOR 98 DEG INCLINATION ONLY

- SHADED AREAS REPRESENT PRIMARY REGIONS AFFECTED BY PROGRAM VARIABLES. PAYLOADS REQUIRING PERFORMANCE IN THESE REGIONS SHOULD VERIFY CAPABILITY WITH JSC AS EARLY AS POSSIBLE
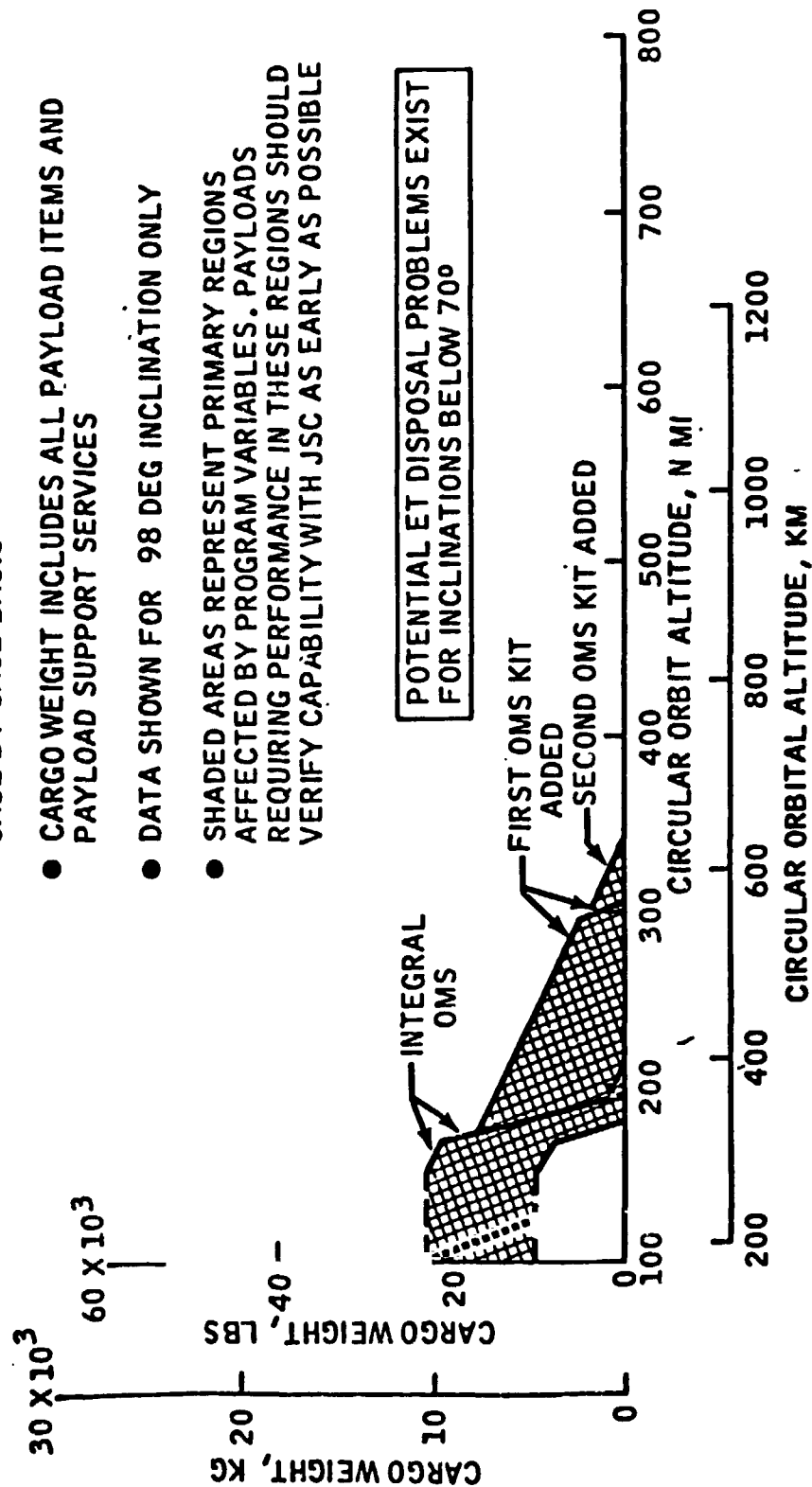
INTEGRAL OMS

FIRST OMS KIT ADDED

SECOND OMS KIT ADDED

POTENTIAL ET DISPOSAL PROBLEMS EXIST FOR INCLINATIONS BELOW 70°

CIRCULAR ORBIT ALTITUDE, N MI

CIRCULAR ORBITAL ALTITUDE, KM

CARGO WEIGHT, LBS

CARGO WEIGHT, KG

FIGURE Ⅴ B-2

MAXIMUM ROUTINE PERFORMANCE OF THE AUGMENTED SHUTTLE
VAFB LAUNCH

UNOFFICIAL

NASA-S-79-3249

- POST 1985 TIME PERIOD
- OMS ΔV RESERVES = 3.3%
- OMS ΔV LAUNCH (100 NMI) = 476 FPS
- NO RENDEZVOUS
- 2σ FRP ON AOA
- MAY 1979 VEHICLE PROJECTION
- NASA REFERENCE MISSION 4 MANIFEST
  (32K LB P/L + FULL OMS + FULL)
  RCS TO 98° INCLINATION

67

1213-81 NASA-S-79-2262 B
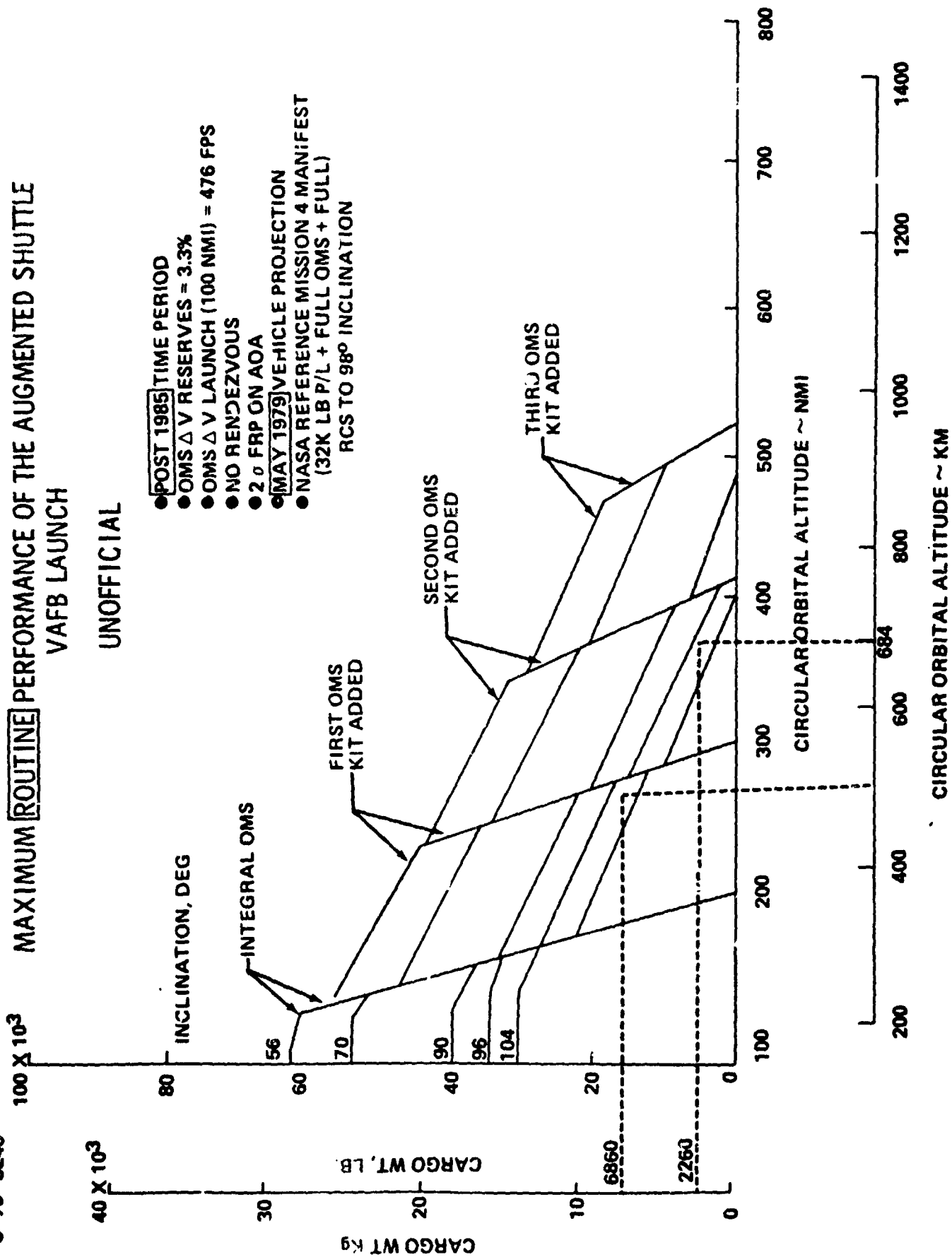
FIGURE V. B-3

NEAR TERM (PRE 1985) CARGO WEIGHT VERSUS CIRCULAR ORBITAL ALTITUDE
KSC LAUNCH, DELIVERY ONLY
UNOFFICIAL
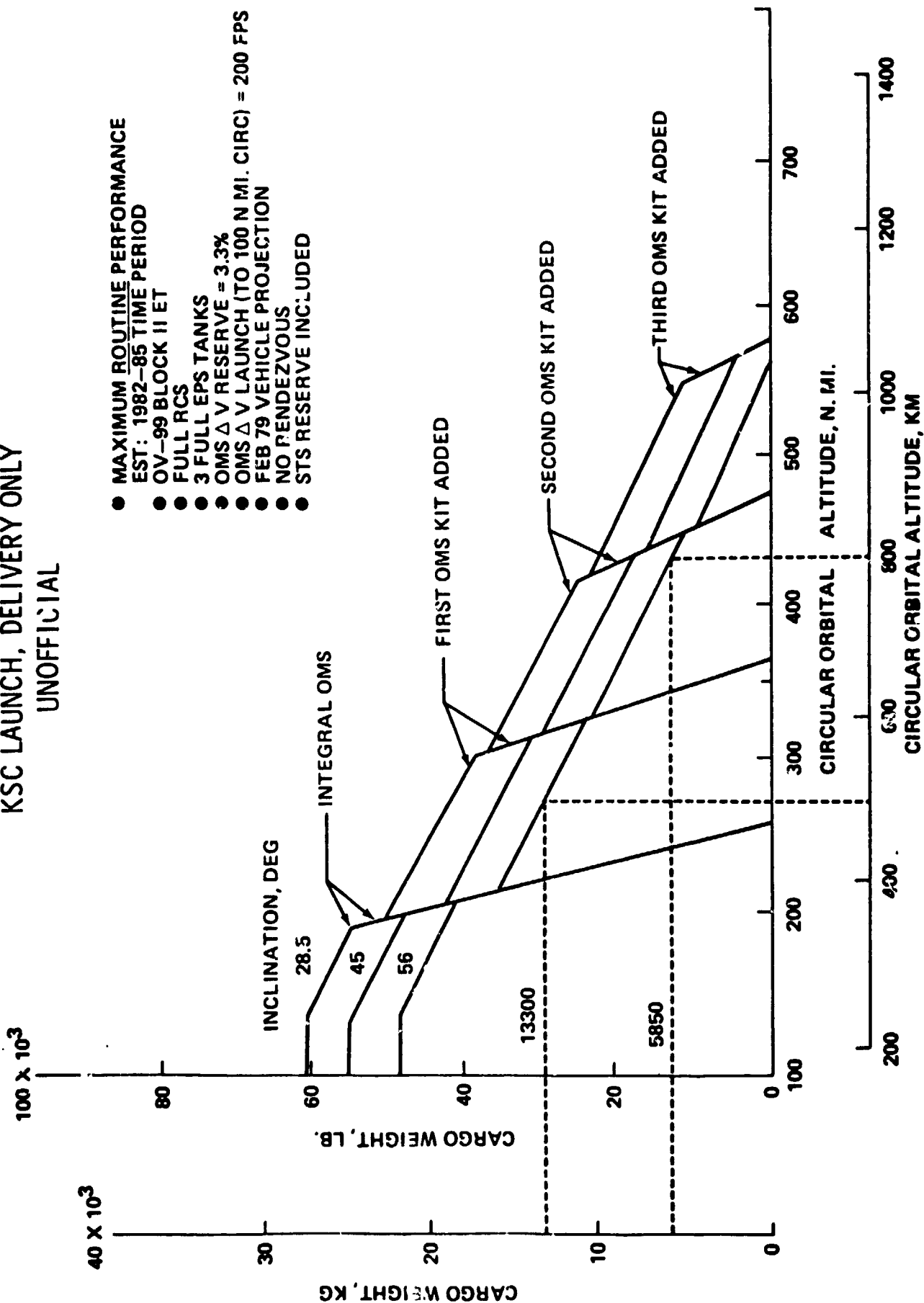
- MAXIMUM ROUTINE PERFORMANCE
- EST: 1982-85 TIME PERIOD
- OV-99 BLOCK II ET
- FULL RCS
- 3 FULL EPS TANKS
- OMS Δ V RESERVE = 3.3%
- OMS Δ V LAUNCH (TO 100 N MI. CIRC) = 200 FPS
- FEB 79 VEHICLE PROJECTION
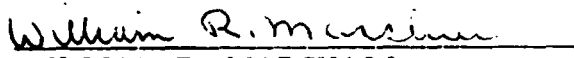- NO RENDEZVOUS
- STS RESERVE INCLUDED

68

APPROVAL

ACCOMMODATIONS ASSESSMENT:
SPACEBORNE DOPPLER LIDAR
WIND MEASURING SYSTEM

The information in this report has been reviewed for security classification. Review of any information concerning Department of Defense or Atomic Energy Commission programs has been made by the MSFC Security Classification Officer. This report, in its entirety, has been determined to be unclassified.

This document has also been reviewed and approved for technical accuracy.

CHARLES R. DARWIN
Director, Preliminary Design Office

WILLIAM R. MARSHALL
Director, Program Development